



HAL
open science

Identification of Oxidized Platinum Single Atoms on Chlorinated Y-Alumina Support by Density Functional Theory Calculations and X-Ray Absorption Spectroscopy

Adrien Hellier, Ana T.F. Batista, Christèle Legens, Antonio Aguilar Tapia, Olivier Proux, Jean-Louis Hazemann, Anne-Sophie Gay, Yves Joly, Céline Chizallet, Pascal Raybaud

► **To cite this version:**

Adrien Hellier, Ana T.F. Batista, Christèle Legens, Antonio Aguilar Tapia, Olivier Proux, et al.. Identification of Oxidized Platinum Single Atoms on Chlorinated Y-Alumina Support by Density Functional Theory Calculations and X-Ray Absorption Spectroscopy. *Journal of Catalysis*, 2024, 429, pp.115212. 10.1016/j.jcat.2023.115212 . hal-04440863

HAL Id: hal-04440863

<https://ifp.hal.science/hal-04440863>

Submitted on 6 Feb 2024

HAL is a multi-disciplinary open access archive for the deposit and dissemination of scientific research documents, whether they are published or not. The documents may come from teaching and research institutions in France or abroad, or from public or private research centers.

L'archive ouverte pluridisciplinaire **HAL**, est destinée au dépôt et à la diffusion de documents scientifiques de niveau recherche, publiés ou non, émanant des établissements d'enseignement et de recherche français ou étrangers, des laboratoires publics ou privés.

**Identification of Oxidized Platinum Single Atoms on Chlorinated γ -Alumina Support by
Density Functional Theory Calculations and X-Ray Absorption Spectroscopy**

Adrien Hellier,¹ Ana T. F. Batista,¹ Christèle Legens,¹ Antonio Aguilar Tapia,^{2,#} Olivier
Proux,³ Jean-Louis Hazemann,² Anne-Sophie Gay,¹ Yves Joly,² Céline Chizallet,¹ Pascal
Raybaud^{1,4,*}

¹ IFP Energies nouvelles, Rond-point de l'échangeur de Solaize, BP3, 69360 Solaize, France

² Institut Néel, UPR 2940 CNRS Université Grenoble Alpes, F-38000 Grenoble, France

³ OSUG, UAR 832 CNRS-Université Grenoble Alpes, F-38041 Grenoble, France

⁴ Univ Lyon, ENS de Lyon, CNRS, Université Claude Bernard Lyon 1, Laboratoire de Chimie
UMR 5182, F-69342 Lyon France

#current address: Institut de Chimie Moléculaire de Grenoble, UAR2607 CNRS Université
Grenoble Alpes, Grenoble F-38000, France

*Corresponding author: pascal.raybaud@ifpen.fr

ABSTRACT

The existence and nature of oxidized Pt single atoms (SA) are unraveled on two γ -Al₂O₃ supported Pt catalysts (0.3 wt%) containing two chlorine contents (0.1 and 1.4 wt%) characterized by HRSTEM and HERFD-XANES/EXAFS after a calcination treatment at 520°C. Pt SA are revealed as PtO_xCl_y complexes where the number of oxygen (x) and chlorine (y) ligands directly depends on the chlorine content. In order to interpret these experimental observations and provide coherent atomic structures for these PtO_xCl_y complexes, the thermodynamic stability of the oxidized Pt SA species supported on the (100) surface model of γ -Al₂O₃ is determined by density functional theory (DFT) as a function of the calcination conditions determined by the temperature, and partial pressures of H₂O, HCl and O₂. It is shown that various ligands such as Cl, OH, O (from the alumina surface or as extra-ligands) and H₂O are coordinated to Pt depending on the conditions and chlorine content. Various square planar and square-based pyramidal PtO_xCl_y species such as PtO₂, PtOCl₂, PtCl₄ are found to be stable in calcination conditions, while octahedral Pt(OH)_xCl_{4-x}(H₂O) are stabilized in XAS recording conditions. The feature of these DFT simulated octahedral Pt SA species are successfully compared to XAS data. On one hand, based on thermodynamics arguments we proposed models of supported complexes in agreement with EXAFS coordination number and distances (Pt-O, Pt-Cl and Pt-Al). On the other hand, the simulated XANES spectra at the Pt L₃ edge for these complexes match well with the experimental HERFD-XANES and reveal that the bump feature observed between 11575 eV and 11585 eV (post-edge signal) is a tracer of the amount of Cl coordinated to Pt SA.

Keywords: platinum, single atom, alumina, chlorine, calcination, DFT, EXAFS, HERFD-XANES

1. Introduction

Single atom catalysts (or SACs) are more than ever in the scope of the scientific community [1–5] not only due to their adequation with today's needs for energetic and resources' use sobriety[1] but also because of their interesting catalytic properties that differ from nanoparticles (NPs) or bulk metal.[3] Indeed, while they offer an elegant solution in line with the atom economy concept to the use of scarce resource such as the transition metals usually used in catalysis, they also allow new reactivities. This is due to, among other reasons, the exacerbated impact of the support which can tune active site properties similarly to ligands in homogeneous catalysis.[1] However, because of thermodynamic reasons single atoms tend to sinter, making their stabilization highly challenging. Cluster and nanoparticles have been known for decades to be attractive metallic catalysts, but thanks to the progress made in high-resolution microscopy techniques, it is now known that they sometimes co-exist with single atoms.[6,7] Thus, understanding how to control the genesis of the active phase is at the heart of many research works among the scientific community,[8,9] with several challenges to overcome, in particular that of the observation of single atoms, and of the definition of the metallic coordination sphere. As an example, a recent study points out the difficulty for characterization techniques such as X-ray Absorption Spectroscopy (XAS) to quantitatively and accurately determine the proportion of single atom in catalysts.[10]

In 1949, Haensel et al.[11] proposed the use of a very low loading of Pt supported on alumina for catalytic reforming reactions and showed that using a small quantity of an expensive noble metal such as Pt could make it an economically attractive catalyst. Even if we might deviate from the SAC definition, the control of the final state of the active phase was already primordial to optimize the activity of the catalyst. Next developments then made Pt/ γ -Al₂O₃ a major actor among model and industrial heterogeneous catalysts with numerous applications in refining,

petrochemistry, pollution abatement, biomass conversion, plastic recycling, inter alia.[9,12–16] Since the earliest work on Pt/ γ -Al₂O₃ by Haensel et al.[11] numerous works have set to optimize this system, exploring the modification of the support [17–19] or the use of multimetallic catalysts [20–22] to increase the selectivity, resistance, or lifetime of the catalyst.[16,23] Despite the tremendous advances done during these decades, key questions regarding the evolution of the platinum species (dispersion, local structure, interaction with the support) during the catalyst preparation remain unanswered.

Controlling the chemical state and physical dispersion of the Pt/ γ -Al₂O₃ active phase is usually done during its preparation. In the case of Pt/ γ -Al₂O₃ used in catalytic reforming units, preparation usually involves several steps.[16,24–26] The impregnation of oxidized platinum precursors [27], usually chlorinated for naphtha reforming applications,[28–30] is followed by various possible thermal treatments such as drying, calcination and reduction under H₂ to finally obtain a metallic Pt. The presence of chlorine in the precursor serves a dual interest. While it increases the acidity of the support,[31] and by consequence the activity of the bi-functional Pt/ γ -Al₂O₃ catalyst,[32] chlorine is also responsible for a higher platinum dispersion.[6,7,33] This latter effect comes in play in the synthesis but also in regeneration steps such as oxychlorination.[34–36] It was recently observed that the SA/NP ratio after reduction increases with the amount of chlorine in the system.[6,37] However, to the best of our knowledge, chlorine promoted ‘dispersive’ mechanisms remain unknown. In the other hand, the role of chlorine is not always beneficial, and in the case of oxidation reactions, the presence of chlorine in the system leads to lower catalytic performances.[37–40]

The calcination step is of primordial interest as it dictates the state of platinum that will undergo further activation processes such as reduction. Thus, a refined understanding of platinum state after calcination could enhance our capacity to tune efficiently the catalyst. After calcination,

Pt is expected to be mainly under the form of oxidized single atom, or eventually of oxidized oligomers (small clusters)[7,41–45] depending on the Pt loading. As it could be expected from the mono atomic nature of platinum, the support is of primordial importance. Its impact on the highly dispersed phase of the platinum was reported by Bradley et al.[44] and Lee et al.[45] who observed that Pt aggregation was refrained by the strength of the Pt-support interaction. Lambert et al.[46] proposed that the support was not only able to impact the aggregation level of the Pt, but also its coordination sphere with an hypothesis made on self-reduction of $\text{Pt}^{4+}[\text{Cl}]_4$ into Pt^0 being possible on SiO_2 but not on Al_2O_3 due to the interaction of PtCl_x species with the support. Other authors[47,48] found results in line with Lambert's proposal in presence of chlorine during calcination. By using temperature programmed reduction (TPR) experiments combined with UV analysis, Liekse et al.[49] and Liezt et al.[50] suggested that the nature of Pt species was either $\text{PtCl}_x(\text{OH})_y$ or PtCl_xO_y when chlorinated precursors or HCl post-treatment were used or $\alpha,\beta\text{-PtO}_2$ otherwise. More recently, EXAFS experiments on $\gamma\text{-Al}_2\text{O}_3$ supported catalysts with various Pt loadings, Cl loadings, and calcination temperatures, confirm the presence of Cl and O in the coordination sphere of Pt.[7,33,40] A synergetic behaviour of chlorine and oxygen to redisperse the platinum species can be suspected as the presence of both elements is profitably used for oxychlorination processes applied to regenerate naphtha reforming catalysts.[34–36,40,47,49,51]

In the present contribution, we aim at elucidating the precise nature of oxidized platinum species supported on $\gamma\text{-Al}_2\text{O}_3$ after calcination, including the role of chlorine, due to the relevance of this catalytic system, and to the lack of precise knowledge in that respect.

Density functional theory (DFT)[52,53] is a relevant method to provide an atomic scale description[54,55] of such Pt species by combining energetic, electronic and structural insights. Hence, numerous DFT studies have been devoted to supported platinum systems, in particular

on γ -Al₂O₃ in oxidizing atmosphere. Generally speaking, a strong size effect was observed in terms of interaction strength between platinum species and oxygen,[43,56,57] the smaller entities interacting more strongly with O₂. Sangnier et al.[57] studied the absorption of O₂ on Pt₁₃/ γ -Al₂O₃ clusters and demonstrated the key role of bridging interfacial oxygen atoms to anchor the cluster to the surface aluminum atoms. Dessal et al.[43] predicted that the formation of oxidized cluster such as Pt₁₃O₂₂ from PtO₄ was unlikely to happen during calcination. Similarly to Sangnier et al.[57], they attributed to O₂ a stabilizing role on SA through the formation of strong Pt-O-Al bonds. However, no chlorine was considered in these studies. Our previous theoretical work[58] was dedicated to the study of isolated (unsupported) PtO_xCl_y(OH)_z(H₂O)_n expected to form under oxidative and reductive atmosphere mimicking calcination conditions. Through first principles thermodynamics (considering various DFT functionals and beyond), we assessed the combined role of water and chlorine on the most stable species according to experimental conditions and revealed the stability of PtCl₄ or PtO₂ species, only. However, no PtO_xCl_y species was found to be stable as expected experimentally and afore mentioned. Hence, it appeared critical to investigate how the presence of the support (not previously considered) impacts this result. Zhou et al.[59] considered the role of chlorine during the redispersion of platinum supported on γ -Al₂O₃ by using DFT. They proposed that chlorine facilitates the redispersion of Pt through the formation of an oxychlorinated complex PtCl₂(OH)₂ that interacts more strongly with the Al₂O₃ (110) surface than a purely oxidized PtO₂ complex. However, the relevance of such a dehydroxylated and dechlorinated Al₂O₃ (110) surface is highly questionable in these conditions, if we refer to former DFT studies. [31] Moreover, the diversity of oxychlorinated Pt species is much wider and cannot be restricted to PtCl₂(OH)₂ alone as it will be shown in the present work.

Hence, to the best of our knowledge, no theoretical work has been dedicated to the description and the evolution of the experimentally observed oxychlorinated Pt SA during calcination. The aim of this work is thus to investigate by a combined XAS and DFT approach the nature of γ - Al_2O_3 supported single atom platinum under calcination conditions in order to assess the impact of chlorine used in the preparation. Such symbiotic approach resonates with the recent work of Finzel et al.[10] highlighting the limitation of XAS techniques to characterize SA. In the present work, the catalysts are prepared by using a H_2PtCl_6 precursor deposited on a γ - Al_2O_3 support and submitted to calcination. To enhance the formation of Pt SA, the Pt content is as low as 0.3 wt% Pt. To explore the effect of chlorine, two Cl contents (0.1 and 1.4 wt%) are considered. The two samples are characterized by both High Energy Resolution Fluorescence Detected (HERFD)-X-ray Absorption Near Edge Structure (XANES) and Extended X-Ray Absorption Fine Structure (EXAFS) techniques. For the DFT study, a large set of $[\text{Pt}_1\text{O}_x\text{Cl}_y(\text{OH})_z(\text{H}_2\text{O})_n]^0$ complexes are simulated on various sites of the (100) surface of γ - Al_2O_3 where their Cl and O coordination sphere is tested through Gibbs free energy calculations as a function of the external conditions (T, $P(\text{O}_2)$, $P(\text{H}_2\text{O})$, $P(\text{HCl})$). The comparison of DFT results with XAS experiments is undertaken through the analysis of coordination numbers and bond lengths of DFT models to make the bridge with EXAFS data and through the explicit simulation of the HERFD-XANES spectrum. Thanks to this multi-technique approach, we propose a mapping of the species present at an unequalled level of precision in terms of definition of nature of coordination sphere of platinum.

2. Methods

2.1 Catalysts preparation

The two catalysts samples were prepared using the same protocol as described in ref.[6] by diffusional impregnation of γ -Al₂O₃ extrudates ($S_{\text{BET}}=183 \text{ m}^2 \text{ g}^{-1}$ by N₂ physisorption) prepared from PuralSB3™ commercial boehmite powder from Sasol with a H₂PtCl₆ and HCl solution, followed by drying overnight and finally calcination at 520 °C for 2 h under dry air (heating 5 °C min⁻¹, 1 L min⁻¹ g_{cat}⁻¹). The platinum loading was 0.3 wt%. For the 1.4 wt% Cl samples, the chlorine loading was increased by thermal treatment at 520 °C by adding dichloropropane (C₃H₆Cl₂) to the air flow in the proportion of 1 wt% per gram of catalyst, which decomposes into HCl, H₂O and CO₂, generating a HCl partial pressure that allows for the exchange of surface hydroxyls with HCl. For the 0.1 wt% Cl samples, the chlorine loading was decreased by dechlorination, by injecting 8000 ppm of water into a dry air flow (1 L min⁻¹ g_{cat}⁻¹) at 520 °C. The H₂O partial pressure shifts the surface species equilibria to form surface hydroxyls and gaseous HCl.[31]

2.2 XAS characterization

Pt L₃-edge XAS spectra, including both EXAFS and HERDF-XANES spectra, were acquired at the FAME-UHD beamline[60] at the ESRF (Grenoble, France). The beamline is equipped with a liquid nitrogen-cooled double-crystal Si(220) monochromator surrounded by two Rh-coated mirrors for harmonic rejection. The beam size on the sample was kept constant during an energy scan at around 220x100 μm (HxV, FWHM). The [660] reflection of three Ge(110) spherically bent crystal analyzers (bending radius of 1 m) from the multicrystal spectrometer installed at BM16 was used to select the L α 1 (L3-M5) fluorescence line at 9442 eV. The total energy resolution of the HERFD-XANES data was 1 eV determined by the FWHM elastic peak.

Energy calibration of the incoming radiation was performed prior to the measurements by recording the L3-edge transmission spectrum of a Pt foil and assigning the maximum of the first derivative peak to 11564 eV. A Helium bag was placed between the sample, the crystals and the detector to prevent signal intensity loss by absorption of the (fluorescence emitted) X-rays by air molecules. The grinded oxide catalyst samples were packed in quartz Mark-tubes (10 μm wall thickness) for acquisition. Reference compounds were platinum oxide PtO₂ (Sigma-Aldrich, purity >99.9%, CAS Number 52785-06-5) and metallic platinum powder (Strem Chemicals, purity >99.9%, CAS Number 7440-06-4). Data were processed and EXAFS spectra were fitted using Athena and Artemis, respectively, from the Demeter 0.9.26 software package (SI 1).[61] The EXAFS spectra of references PtO₂ was used to obtain S_0^2 .

FEFF6 module in Demeter package was used to generate the paths files further considered in the simulation. Only single scattering up to 4.0 \AA with sufficient ranking (>5%) were taken into account to model the O, Cl, Al and Pt summed paths. For the reconstructed paths, S_0^2 was set to 0.88 as obtained when fitting the PtO₂ reference, while Δr was set to 0. Debye Waller factors were taken at 0.002 \AA^2 for all scatterers on the ΔR range.

2.3 DFT calculations

Energy calculations

The calculations were performed by using the VASP 5.4.1 software.[62,63] Geometries were optimized using the PBE[64] generalized gradient approximation (GGA) exchange correlation functional, and corrected for the dispersion forces with the dDsC[65,66] scheme. A 400 eV cut-off was used for the kinetic energy of the plane wave basis set. Calculations were done at the Γ -point of the Brillouin zone due to the large supercell used: 16.71 x 16.79 x 21.80 \AA^3 . Core electrons were treated by using the projector augmented wave (PAW) formalism.[67] Spin

polarization was considered to define the ground state of each structure. Energies were recalculated after applying a dipolar correction along the z axis (perpendicular to the slab). A Gaussian smearing of 0.05 eV was applied and charges were evaluated using the Hirshfeld[68] formalism. Convergence criteria were fixed to 10^{-7} eV for SCF cycles and to 10^{-2} eV \AA^{-1} for forces. If several isomers exist, the most stable geometry at 0 K was kept for the given stoichiometry. Frequencies have been computed on the previously optimized structures using the finite difference method as implemented in VASP using the central difference scheme with a 0.01 \AA step to ensure the stable, or meta-stable nature of the models and for calculating the vibrational component of the Gibbs free energies.

The impact of the functional on these supported systems is assessed by computing electronic energies using an HSE06[69–71] exchange correlation functional. Due to the computational cost of such calculation, a single point evaluation was done on the geometry and spin state previously optimised at PBE-dDsC level. Because of the minimal impact of the dipolar correction along the z-axis observed at the PBE-dDsC level, they were not considered for HSE06 calculations.

The (100) surface of $\gamma\text{-Al}_2\text{O}_3$ (**SI 2**) as proposed by Digne et al.[72,73] according to the bulk model of Krokidis et al.[74] was used. The surface was considered dehydrated as calculated by Pigeon et al.[75] at the PBE[64]-dDsC[65,66] level which is consistent with the calculations of Digne et al.[72] at the PW91 level. The first two layers were relaxed, in addition to the supported Pt complexes.

Reactions simulated during calcination

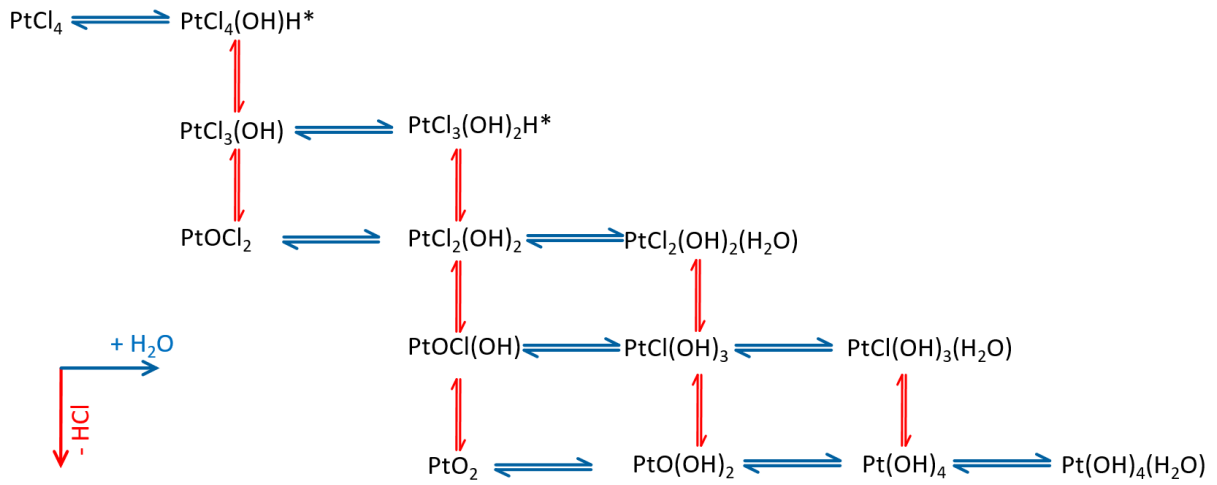
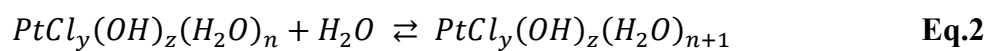
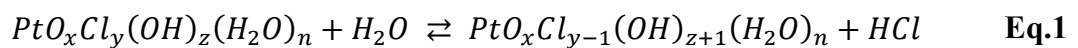
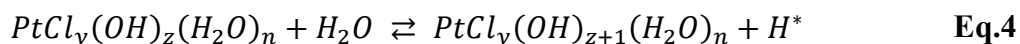
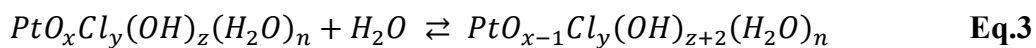


Figure 1. Platinum complexes considered in the thermodynamic model and the interconnected reactions: hydrations, HCl release and ligand exchange. The ligand exchange reaction discussed in the text can be considered as a combination of red and blue arrows.

In the same spirit as proposed in our previous study,[58] we considered that the exchange of a Cl by a OH ligand occurs according to the general equations involving H₂O/HCl in the medium (**Eq. 1**). Hydrations were modelled through three different equations (**Eq. 2-4**). **Eq.2** represents a water molecule added to the coordination sphere of the platinum without dissociation, while **Eq.3** represents a water molecule dissociatively adsorbed on Pt and forming two new hydroxyls on the Pt complex (one involving an oxo ligand). Finally, **Eq.4** stands for water dissociative adsorption leading to two hydroxyls: one on the Pt complex and the other one on the alumina surface, coming from the transfer of a proton to a surface O site (labelled as H^{*}). These equations were also used to link all the considered species (summarized in **Figure 1**) in the thermodynamic diagrams presented in the next section.





Thermodynamic stability determination

The thermodynamic stability of supported platinum complexes under various calcination conditions was determined by calculating Gibbs free energies. Translational, rotational and vibrational contributions were calculated under the rigid-rotor and harmonic oscillator approximation and added to the electronic energy for the gas phase molecule while only the vibrational contributions were considered for the supported systems. For every system, zero-point energy was added. The surrounding environment was treated as an ideal gas phase reservoir. The vapor/liquid water equilibrium was reported on all thermodynamic diagrams to recall the limit of stability of water vapor used in our thermodynamic model. Both PBE-dDsC and HSE06 electronic energies were used to compute stability of platinum complexes during calcination, but independently of the exchange correlation functional used for energies, frequencies calculations were done at the PBE-dDsC level. Calcination was modelled with O₂ as oxidative agent, as it is usually done under air flow,[7,43] and for a temperature of 800 K. During the calcination step, various reactions such as dehydration or ligand exchange are experimentally expected.[7,50] These reactions were simulated by considering variable pressures of H₂O and HCl, knowing that for calcination H₂O pressure is close to 1x10⁻⁶ bar. Due to experimental protocols, the HCl pressure is rarely measured during calcination processes, while the water pressure is known. Hence, the HCl pressure will be used here as a variable adjusting the chlorine contents in the system.[31] Thus, we used a set of HCl pressure values : 0 for the chlorine free case, 10⁻¹² and 10⁻⁶ bar. We allow P(H₂O) to vary between 10⁻¹² and 1 bar, while temperatures were allowed to range from 0 K to 1000 K.

2.4 XANES simulations

The ab initio XANES simulation at platinum's L_3 -edge was undertaken using the FDMNES package developed by Joly et al.[76,77] The package calculates self-consistently the electronic structure of a given structure in real space using DFT. The calculation of XANES spectra required the knowledge of all the final states up to a certain energy. In this part, the LDA exchange correlation functional parametrized by Hedin and Lundqvist[78] was used and final states were calculated by solving the Schrödinger equation with finite difference method (FDM).[79] Despite being more computationally expensive than the multiple scattering theory that relies on the Muffin-tin approximation,[79] using the finite difference method allows to get rid of any approximation on the shape of the potential and is thus more accurate. Considering Pt as a heavy atom, fully relativistic calculations were undertaken, and spin orbit coupling was accounted for. Better agreement with experimental spectra was obtained after considering that the absorbing atom was excited, that is with a core-hole in the $p_{3/2}$. Convolution parameters were chosen to get best agreement with experimental spectra. Most parameters were let as default while core level width was fixed at 1.1 eV (Γ_{hole}) and the maximum width of the final state fixed at 8 eV (Γ_{max}). Pt L_3 -edges calculations were performed first for the reference Pt_{bulk} spectrum using the fcc structure (bulk parameter of $a = b = c = 3.9239 \text{ \AA}$ and $\alpha = \beta = \gamma = 90^\circ$) and within a 7 \AA radius sphere centred on one Pt atom. A slightly lower 6 \AA radius was used for the supported Pt models. The core hole effect makes that LUMO are shifted down by a constant value of -1 eV compared to the Fermi level calculated during the SCF procedure (SI. 3).

For Pt bulk the shift was up to -4 eV to get a better agreement with experimental Pt's L₃ spectra. Then, both white lines (WL) of experiment and simulation of Pt bulk were aligned, and the shift needed to achieve it was applied to all calculated spectra. Finally, the intensity of all calculated spectra was multiplied by a constant factor such that the post-edge regions of both Pt_{bulk} spectra are equal. In order to quantitatively compare the XANES simulations with the experimental spectra of calcined catalysts, linear combination of calculated spectra was calculated using the CVXPY[80,81] library after discretizing the calculated spectra over the same energies than the experimental ones.

3. Results

3.1 HERFD-XANES analysis

Figure 2 shows that the two HERFD-XANES spectra of the two calcined γ -alumina supported Pt samples significantly differ from the bulk Pt and PtO₂ sample references. Both γ -alumina supported Pt samples exhibit a white line (WL) shifted to higher energies than the one of bulk Pt and PtO₂. Moreover, a slight shift of the WL to higher energy is found for the sample with low Cl content with respect to the high Cl content. In addition, a subtle difference between the two spectra can be observed at ~15580 eV where a bump is present. The bump's intensity is slightly more pronounced in the case of the 1.4 wt.% Cl sample than for the 0.1 wt.% Cl. This bump is not present for the reference PtO₂. A deeper understanding of this phenomenon will be provided in the discussion section by simulating the XANES spectra for the most relevant DFT molecular models of the catalysts.

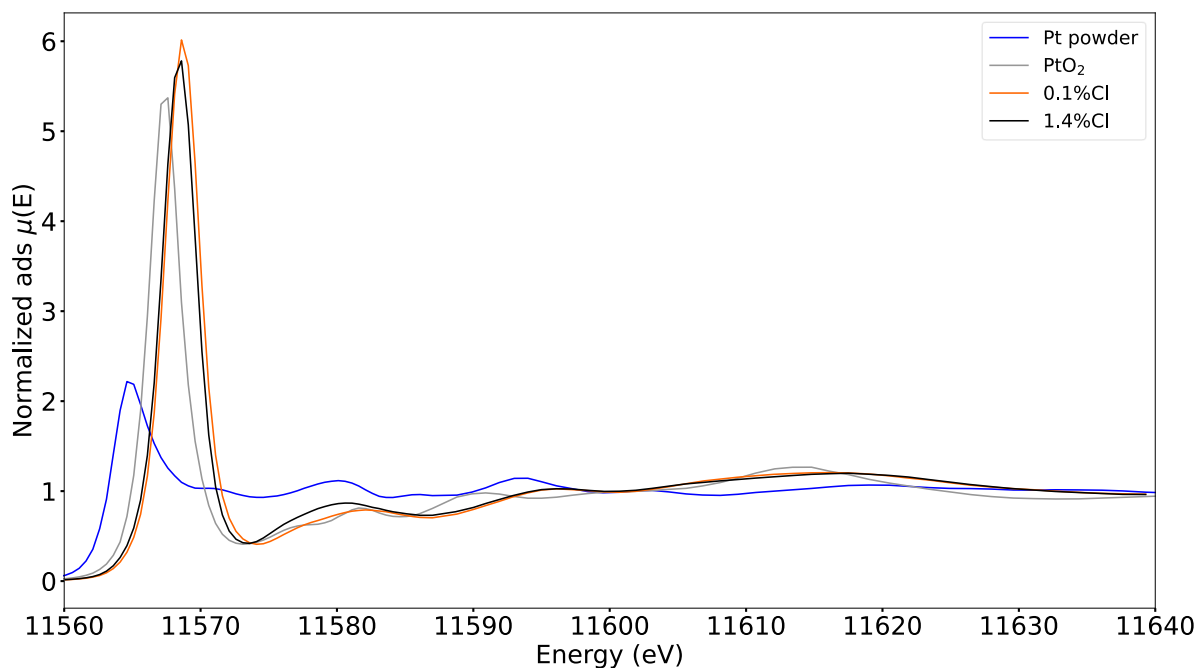


Figure 2. Pt L_3 -edge HERDF-XANES spectra of reference PtO_2 and metallic Pt powders in addition of calcined samples: 0.3 wt.% Pt supported on γ -alumina with 0.1 and 1.4 wt.% Cl.

3.2 EXAFS analysis

The EXAFS spectra and the wavelet transform analysis are presented in **Figure 3, a-c)** for the sample with low chlorine content (0.1 wt.%Cl). The corresponding imaginary part is reported in **Figure S2 a)**. The parameters used for the best fit shown in **Figure 3** are reported in **Table 1**, while fits for the reference Pt powder and PtO_2 are reported in **SI.1**. Two main regions can be distinguished in the $|\chi(R)|$ spectra (**Figure 3**): one from 1.3 to 2.3 Å and a second one from 2.3 to 3.3 Å. The continuous Cauchy wavelet transform[82] (CCWT) analysis suggests that the first region should correspond to one main light scatterer with possible contribution of a second one. The 1.3-2.3 Å region can thus be fitted with a Pt-O path and a Pt-Cl path, with oxygen being the main neighbor in the 1st shell. Indeed, the dechlorination process removes the chlorine and substitutes the attached Cl with O resulting in an oxygen rich $PtCl_xO_y$ oxide complex. However, the contribution of the Pt-Cl path cannot be ignored. Even with a lengthy

dechlorination protocol, the remaining chlorine stays in the oxide complex, leading to a neighboring environment distinct from the one found in Pt/Al₂O₃ samples prepared from non-chlorinated precursors.[40,43,83,84]

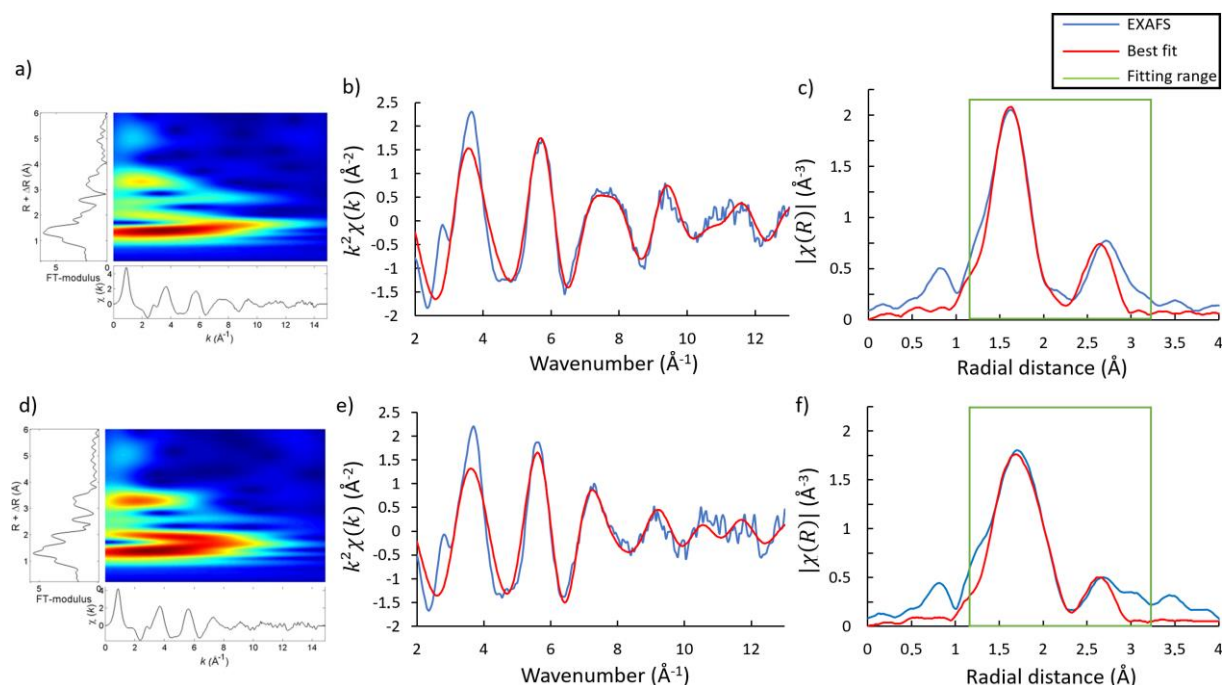


Figure 3. EXAFS results for 0.3 wt.% Pt supported on γ -Al₂O₃ at 0.1 wt.% Cl (a-c) and 1.4 wt.% Cl (d-f). a) and d) CCWT analysis,^[82] b) and e) EXAFS $k^2\chi(k)$ oscillations, c) and f) magnitude of the Fourier transform $|\chi(R)|$ (no phase correction), all weighted by k^2 . In b), c), e) and f), the red line represents the best fit using Al in the second shell. In c) and f), the fitting range is represented by the green frame.

Fitting the 2-3 Å region is less straightforward. However, not considering this region, the fit would not correctly reproduce all the main features of $\chi(k)$. The position of the second region could be compatible with the signal originating from various possible Pt-X distances where X means Al, O or even Pt itself. Nevertheless, the wavelet analysis clearly indicates that this region is a light scatterer (even when k^3 -weighted data are used). This explains why it is impossible to adjust this region by using platinum as second neighbor in the EXAFS fit, with Pt-Pt distance initiated from Pt-Pt distances found in PtO₂ reference phase. Indeed, $k^2\chi(k)$

oscillations reported in Figure S3 a) (using Pt in the second shell) reveal a clear discrepancy between experimental and the fitted spectrum for large k number where Pt-Pt contribution is predominant. Simultaneously, the second region of the modulus is not correctly recovered, due to the too large Pt-Pt distance. This leads to large R-factor value (0.09). This indicates that oxidized platinum complexes are atomically dispersed. The 2.3-3.3 Å region was thus treated as a 2nd shell light scatterer (Al or O, Table 1) leading to more reasonable R-factor values (close to 0.04).

0.3 wt.%Pt supported on γ -alumina with Cl contents	k-range (\AA^{-1})	Path	Coordination number	R (\AA)	σ^2 (\AA^2)	ΔE_0 (eV)	R-factor
0.1 wt.%Cl 2 nd shell: Pt-O _{long}	4.0 – 11.7	Pt-O	5.2±0.6	1.98±0.01	0.002±0.001	9.6±1.9	0.04
		Pt-Cl [#]	0.8±0.6	2.29±0.03			
		Pt-O _{long}	5.5±3.4	3.05±0.04	0.002±0.007		
0.1 wt.%Cl 2 nd shell: Pt-Al	4.0 – 11.7	Pt-O	5.6±0.5	1.98±0.02	0.002±0.001	11.6±1.2	0.04
		Pt-Cl [#]	0.4±0.5	2.26±0.04			
		Pt-Al	3.1±1.8	2.91±0.03	0.002±0.006		
1.4 wt.%Cl 2 nd shell: Pt-O _{long}	3.6 – 11.8	Pt-O	3.9±0.5	2.00±0.02	0.003±0.001	10.7±1.0	0.04
		Pt-Cl [#]	2.1±0.5	2.28±0.02			
		Pt-O _{long}	3.9±2.5	3.09±0.05	0.003±0.008		
1.4 wt.%Cl 2 nd shell: Pt-Al	3.6 – 11.8	Pt-O	4.1±0.5	2.01±0.02	0.002±0.001	11.4±0.8	0.04
		Pt-Cl [#]	1.9±0.5	2.29±0.02			
		Pt-Al	1.9±1.6	2.95±0.03	0.002±0.008		

Table 1. EXAFS fitting results for oxide catalysts at 0.1 and 1.4 wt.% Cl considering either a 2nd shell Pt-O_{long} or a 2nd shell Pt-Al coordination. $E_0=11566.1$ eV; $1.15 < R < 3.2$ Å; $N_{ind}=12$; $N_{var}=8$. #Pt-Cl coordination number is evaluated imposing $N_{PtCl}+N_{PtO} = 6$ after verifying that smaller values for the total coordination number of Pt are not appropriate.

A second shell Pt-O contribution with a distance of 3.3 Å was reported in the literature[85] for 1wt.% Pt and 10 wt.% Pt/ γ -Al₂O₃ catalysts calcined at 300 °C. It was found that using paths obtained through the quick first shell (QFS) tool of the Artemis software, setting a path distance of 3.0 Å, here called Pt-O_{long} or Pt-Al, resulted in fits of a reasonable quality as shown in **Table 1**. The fit shown in **Figure 3** was done by using Pt-Al. It was not possible to discriminate

unambiguously between these two scatterers, O or Al. Also, using both did not improve the fit. The 2nd shell parameters vary depending on the scattering atom: CN of Pt-O_{long} is higher and Pt-Al atomic distance is slightly shorter. As we will discuss it latter by considering DFT results, the 2nd shell scatterer, be it O or Al, is due to the alumina support and it reveals Pt precursor-alumina interactions.

For the higher Cl content (1.4 wt.%, **Figure 3, d-f**) the wavelet analysis indicates clearly that there are two 1st shell light scatterers. Accordingly, in the magnitude spectra of the Fourier transform, the signal between 1.3 and 2.3 Å is broad. Indeed, the $\chi(k)$ is distinct from what was obtained for the catalysts with 0.1 wt.% Cl, particularly after 6 Å⁻¹. At 1.4 wt.% Cl, the coordination number for the Pt-Cl path is enclosed between 1.9 and 2.1, indicating that the surface oxide complex PtCl_xO_y is enriched in chlorine with respect to the sample at 0.1 wt.% Cl. Regarding the Pt-Cl distance, it remains rather similar (around 2.28 Å) for the two samples at 0.1 wt.% Cl and 1.4 wt.% Cl. The signal in the 2.3 – 3.3 Å region was treated as a 2nd shell with a light scatterer, considering either Pt-O_{long} or Pt-Al (**Figure 3**). As in the previous case, any attempt to use Pt-Pt contribution (initiated from a PtO₂ reference phase) was unsuccessful.

In summary, the fitting of EXAFS data for the oxide samples at 0.1 wt.% Cl and 1.4 wt.% Cl suggests that platinum should be mostly atomically dispersed in the form of an oxygen rich PtCl_xO_y complex. After checking different hypothesis for the overall Pt coordination number, fixing it at a value of 6 was found to be the most appropriate. Being coordinated to 6 ligands, we further found that CN(Pt-O)≈5 and CN(Pt-Cl)≈1 for 0.1 wt.% Cl and CN(Pt-O)≈4 and CN(Pt-Cl)≈2 for 1.4 %Cl. Hence, no Pt-Pt or Pt-O-Pt contributions were found for the first or second shells. This finding is consistent with high resolution scanning transmission electron microscopy, as illustrated in the case of 0.3 wt.% Pt over γ -alumina with 1.4 wt.%Cl in **Figure S6**, revealing that platinum is well dispersed and well distributed over the support:

predominantly Pt single atoms are found in agreement with previous reports.[7,44] Such samples have been described as single atom catalysts in the literature.[43,44,86] These Pt species are in interaction with the alumina support, as evidenced by the contribution of a long-distance 2nd shell EXAFS signal assigned to either O or Al. This analysis will be further refined with DFT models determined in what follows.

3.3 DFT simulation of the γ -Al₂O₃ supported Pt single atoms

In this part, we describe some relevant structural, electronic and energetic properties of the $[\text{Pt}^{4+}(\text{O}^{2-})_x(\text{Cl}^-)_y(\text{HO}^-)_z(\text{H}_2\text{O})_n]^0$ (with $2x+y+z=4$) complexes supported on the (100) surface of γ -Al₂O₃ that will be used to simulate the calcination process. We propose to compare these properties with similar ones determined for the same complexes recently studied in gas phase [58] in order to underline the subtle interplay between Pt SA complexes and the γ -Al₂O₃ support.

Structural features

The dehydrated (100) γ -Al₂O₃ surface developed by Digne et al.[72,73] exhibits various anchoring sites for the Pt complexes (**Figure 4, a**). Using the same nomenclature as in [72,87], three different oxygens (A, B, C) and three aluminum sites (I, II, III) allow multiple configurations for the adsorption of platinum complexes. A rigorous screening was done for all complexes to determine the most stable anchoring sites. During this exploration, we found a simple relation between the number of ligands in the coordination of platinum and the most favorable adsorption site. Complexes with three or more ligands (excluding the surface atoms) adsorb more favorably with the Pt atom on top of oxygen B (O_B) (**Figure 4, b**). For the PtO₂ complex (with two ligands), an anchoring mode involving two oxygens A (O_A) and C (O_C) is preferred (**Figure 4,c**).

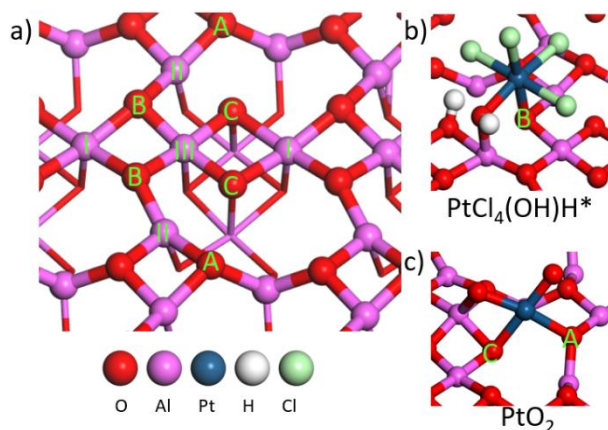


Figure 4. a) Non-equivalent Al and O sites on the (100) γ - Al_2O_3 surface. Most stable adsorption modes of two relevant Pt complexes: b) $\text{PtCl}_4(\text{OH})\text{H}^*$ with a Pt- O_B bond, b) PtO_2 with two Pt- O_A and Pt- O_C bonds. $\text{PtCl}_4(\text{OH})\text{H}^*$ means that the water ligand is dissociated into one OH group as ligand and one proton adsorbed on the alumina surface.

As it could be expected from the single atom nature of platinum, both the coordination sphere and the surface impact the resulting properties of the catalyst and need to be analyzed carefully. **Table S2** and **Figure S7** reports the complete list and description of supported complexes under consideration. As mentioned before, only PtO_2 adsorbs at the O_A and O_C sites, and exhibits a square planar geometry (**Figure S7, n**). All other species adsorb at the O_B site. PtOCl_2 , $\text{PtCl}(\text{OH})$ and $\text{PtO}(\text{OH})_2$ are square planar, O_B playing the role of the fourth ligand (**Figure S7, k-m**). All $\text{PtCl}_y(\text{OH})_{4-y}$ species exhibit square-based pyramidal geometry, but the orientation of the pyramid with respect to the surface varies as a function of y . For $y = 0, 1$ and 3 , the basis of the pyramid is parallel to the surface, whereas it is perpendicular for $y = 2$ and 4 (**Figure S7, a-e**). All other species are octahedral (**Figure S7, f-j**). In all cases, the most stable isomers maximize the number of hydroxyls bridging platinum to surface aluminum atoms.

Upon adsorption, Pt complexes undergo structural changes with respect to their gas phase analogues, and the fluctuation of the Pt-X bonds (X being a ligand in the coordination sphere) depends on the nature of the ligand. The mean Pt-Cl bond length (2.27 Å) is actually unchanged in both supported and gas state[58] respectively, while the average Pt-OH bond elongates from

1.94 Å in gas phase to 2.02 Å for the supported system. Pt-O_{oxo} are more impacted and an elongation of 0.11 Å is calculated between the gas phase (1.74 Å) and the adsorbed species (1.85 Å). By contrast, the platinum-water mean distance exhibits a significant contraction of 0.18 Å with 2.05 Å for the adsorbed complexes against 2.23 Å for the gas phase. Moreover, in some cases, H₂O dissociation occurs, leading to the formation of two hydroxyls, one on the complex and the second on the alumina surface. The two species in question are PtCl₄(H₂O) and PtCl₃(OH)(H₂O), that will be named PtCl₄(OH)H* and PtCl₃(OH)₂H* respectively (* highlighting the dissociation of the proton on the surface). The geometry (square planar, pentahedral or octahedral) of the complex strongly impacts the optimized distances between platinum and the surface. For a given geometry, the Pt-O_{surf} distance generally increases with the number of chlorine ligands. Among the complexes coordinated to the surface by one Pt-O_{surf} bond, the distances range between 1.97 Å for Pt(OH)₄ and 2.11 Å for both PtCl₄ and PtCl₄(OH)H*. During the hydration of the pentahedral PtCl_y(OH)_{4-y} (leading to octahedral complexes) an average elongation of the Pt-O_{surf} bond of 0.044 Å is calculated. The square planar complexes bearing oxo ligands, exhibit rather long Pt-O_{surf} distance with 2.05 Å for both PtO(OH)₂ and PtOCl(OH), and slightly longer for PtOCl₂ with 2.08 Å. While PtO₂ is the closer to the surface due to its double anchoring O site (A and C), its two Pt-O_{surface} bonds are calculated at 2.07 and 2.15 Å with the last bond being the longest among all the considered species (**Table S2**).

Charge analysis

The surface impacts the platinum electronic density through the grafting mode of the complexes with a stronger depletion with increasing number of anchoring sites. This effect of the support is particularly well highlighted by comparing the Hirshfeld charges of the complexes supported

or in gas phase (**Figure 5**). An average difference of +0.071 e is calculated between the supported and gas phase species, which is due to the withdrawing effect of the additional ligand effect of the O_{surf} site which further depletes Pt atom from electrons. The largest difference is for PtO_2 with 0.58 e for Pt if the complex is supported, compared to 0.39 e in gas phase. This may be explained by the fact that PtO_2 is grafted on the support through two $Pt-O_{\text{surf}}$ bonds.

Independently of the adsorption mode of the complexes, oxo ligands are more oxidizing than hydroxyls, being themselves more oxidizing than chlorines (for a fixed number of ligands). This trend was already observed in gas phase.[58] Thus, substituting Cl ligands for OH induces a systematic increase of the platinum Hirshfeld charge. The calculated platinum charge values reported for the 3 couples $PtCl_4 / PtOCl_2$, $PtCl_2(OH)_2 / PtO(OH)_2$ and $PtCl_3(OH) / PtOCl(OH)$ for the same anchoring site (**Table S2, Figure S7**) reveal that one oxo ligand has a similar impact as two chlorine ligands on the platinum charge. The formation of an octahedral complex through the hydration of a pentahedral $PtCl_y(OH)_{4-y}$ (with $y < 3$) complex impacts only slightly the charge of platinum. Surprisingly, this is still true for the two dissociative hydrations ($PtCl_4 + H_2O \rightarrow PtCl_4(OH)H^*$ and $PtCl_3(OH) + H_2O \rightarrow PtCl_3(OH)_2H^*$) despite the addition of a hydroxyl in the coordination sphere instead of a water molecule. For these two cases, we found in the one hand an increase of the oxidative power of the coordination sphere of the platinum but in the other hand we also calculated that the surface is less oxidated (**Table S2**). Overall, these two phenomena compensate each other, leading as for the other hydrations to only small changes to the Pt charge.

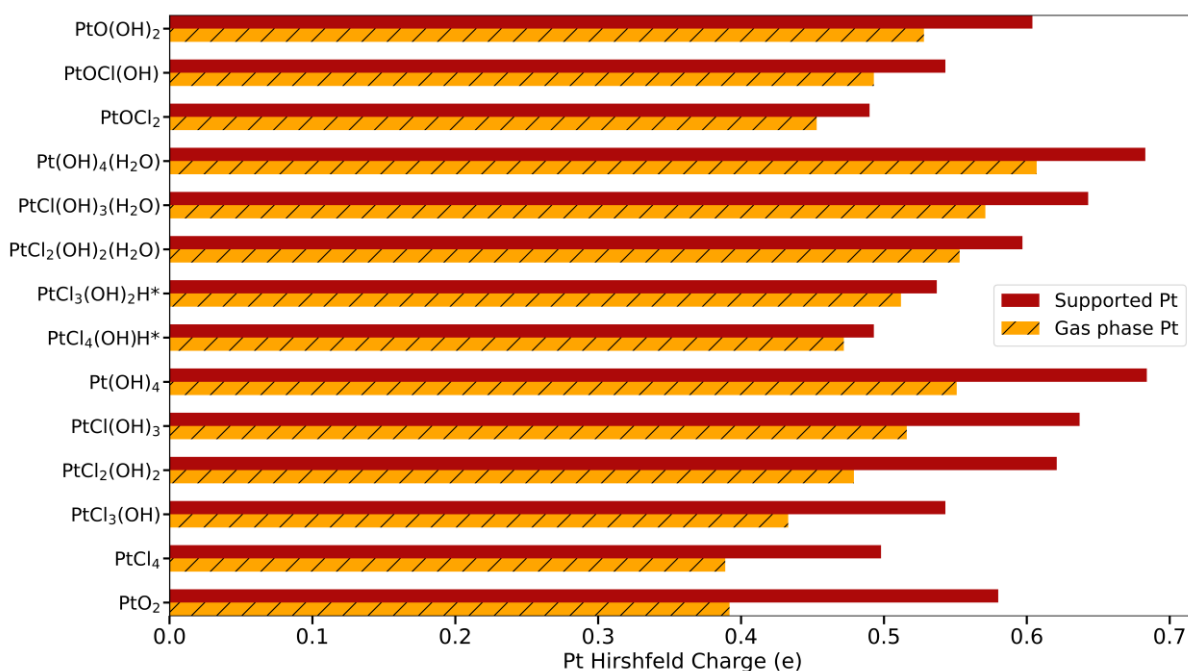


Figure 5. Analysis of the Hirshfeld charges of platinum within various complexes for a given stoichiometry. As described in the method, the water is dissociated into a bridging hydroxyl and proton for $\text{PtCl}_4(\text{OH})\text{H}^*$ and $\text{PtCl}_3(\text{OH})_2\text{H}^*$. Numerical values for the supported complexes are reported in Table S2, while gas phase values are taken from ref.[58]

Thermodynamics of calcination

In this part, we analyze the evolution of the stable species under oxidizing conditions mimicking the calcination step of the catalyst preparation through the determination of thermodynamic diagrams. All the calculated $[\text{PtO}_x\text{Cl}_y(\text{OH})_z(\text{H}_2\text{O})_n]^0$ complexes are linked through the reaction network involving ligand exchanges and hydrations (**Eq. 1-4**) graphically illustrated in **Figure 1**. A detailed analysis of the energetics of these reactions at 0 K is provided in **SI 6**. Details on calculations are reported in section **2.3**.

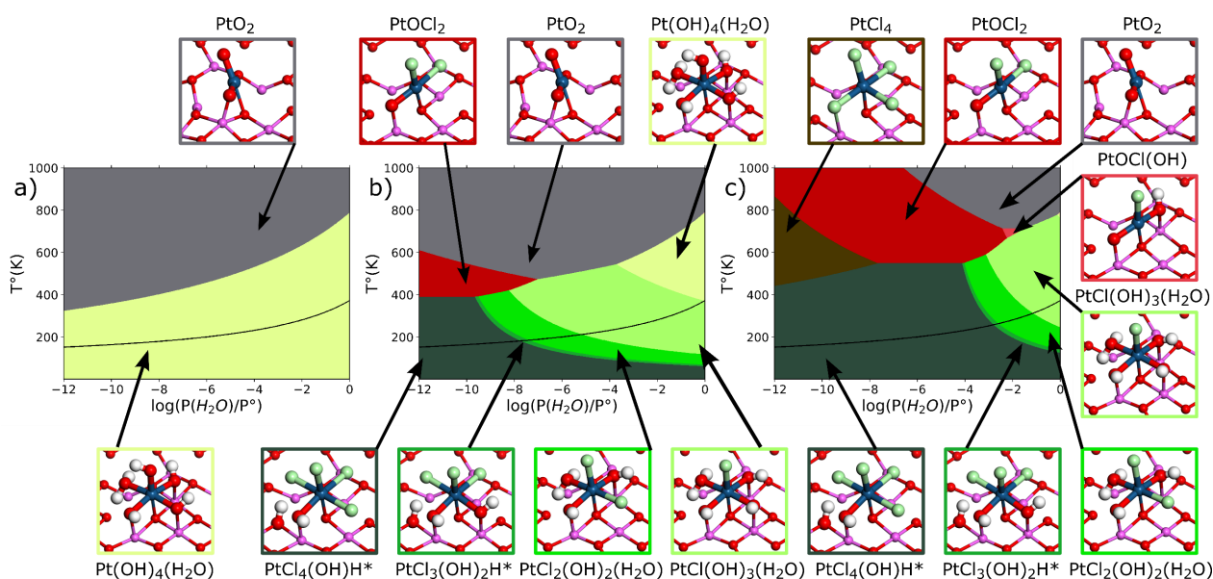


Figure 6. Thermodynamic diagrams of the most stable species under oxidative conditions for three chlorine pressures: a) without chlorine; b) $P(\text{HCl}) = 1 \times 10^{-12}$ bar; c) $P(\text{HCl}) = 1 \times 10^{-6}$ bar. The gas phase domain of water is located above the black curved line representing the liquid/vapor equilibrium. Same color code for structures as in Figure 4.

Figure 6 represents the most stable species (lowest Gibbs free energy of all simulated species) expected in calcination conditions according to the water pressure and temperature for three levels of Cl pressure. In the absence of chlorine only two Pt species are expected, PtO_2 and its hydrated counterpart $\text{Pt}(\text{OH})_4(\text{H}_2\text{O})$. The dehydrated form is expected above 400 K for 1×10^{-6} bar of water (**Figure 6, a**) which is a water pressure usually considered in calcination conditions. As it could be expected from the hydration/dehydration reactions linking these two species, higher water pressure and low temperature (as found in XAS experiments) favors the octahedral $\text{Pt}(\text{OH})_4(\text{H}_2\text{O})$ complex. However, the Pt complex has to migrate from an oxygen (B) to oxygens (A) and (C) during this dehydration reaction (**Figure 4**).

Adding chlorine drastically changes the thermodynamic landscape as exchanging hydroxyls for chlorine ligands was found to be favored (**Table S3**) from an electronic energy point of view. Thus, a great variety of octahedral $\text{PtCl}_y(\text{OH})_{4-y}(\text{H}_2\text{O})$ complexes (H_2O being dissociated or not) bonded to one O atom of the support are stable at low temperatures. Expectedly, the Cl/OH

ratio decreases as the water pressure increases. Chlorine stabilizes the hydrated state of the Pt complexes with a dehydration temperature being slightly higher for the hydroxychlorinated complexes (~ 500 K at 1×10^{-6} bar of water) than for the totally hydroxylated case (~ 400 K at $1 \cdot 10^{-6}$ bar of H_2O) (**Figure 6, a), b) and c)**). However, at a low amount of HCl ($P(HCl) = 1 \times 10^{-12}$ bar), the role of chlorine is not significant enough to impact the high temperatures part of the diagram where PtO_2 is still expected to be the most stable specie, especially for typical calcination conditions ($T \sim 800$ K and $P(H_2O) = 1 \times 10^{-6}$ bar). At low water pressure and intermediate temperature (~ 400 - 600 K), a square planar platinum is stabilized ($PtOCl_2$) and it can be seen as possible intermediate species between the hydrated octahedral Pt complexes and PtO_2 .

Increasing the HCl pressure to 1×10^{-6} bar (**Figure 6, c)**) strongly modifies the diagram at both low and high temperatures. On the low temperature domain the $PtCl_y(OH)_{4-y}(H_2O)$ complexes (already present at $P(HCl) = 1 \times 10^{-12}$ bar, H_2O being dissociated or not) are strongly stabilized. In particular, the fully chlorinated $PtCl_4(H_2O)$ (in the $PtCl_4(OH)H^*$ form) is stable on a larger domain: up to 550 K for $P(H_2O)$ between 1×10^{-8} and 1×10^{-4} bar. The other hydroxychlorinated complexes are still found at higher water pressure but on a smaller domain and the fully hydroxylated $Pt(OH)_4(H_2O)$ vanishes. At higher temperature, the PtO_2 domain is shrunk in favour of $PtCl_4$, $PtOCl_2$ and marginally $PtOCl(OH)$. The square-based pyramidal $PtCl_4$ complex is stable for the lowest water pressure and up to $P(H_2O) = 1 \times 10^{-11}$ bar at $T = 800$ K. Then $PtOCl_2$, a square planar platinum complex, is expected until $P(H_2O)$ reaches 1×10^{-4} bar at 825 K. Finally, the stabilization of PtO_2 should occur for $P(H_2O) > 1 \times 10^{-4}$ bar. These diagrams show the importance of controlling the amount of chlorine in the system as it drastically changes the expected species after calcination. In summary, for typical calcination conditions ($T = 800$ K

and $P(\text{H}_2\text{O}) = 1 \times 10^{-6}$ bar), three species PtO_2 , PtOCl_2 and PtCl_4 appear to be stable depending on the amount of chlorine ($P(\text{HCl})$) present in the system (**Figure S9**).

The role of the support in the stabilization of the platinum complexes is far from being negligible. Indeed, by comparing these calcination diagrams to those determined in gas phase,[58] it is found that the formation of PtOCl_2 is possible only in the presence of the support which stabilizes it by forming a square planar platinum (whereas in gas phase, it is a triangular complex). Moreover, at the low temperatures corresponding to XAS experimental conditions, the support stabilizes various octahedral $\text{PtCl}_y(\text{OH})_{4-y}(\text{H}_2\text{O})$ hydroxy-chlorinated platinum complexes by facilitating successive exchanges of chlorine for hydroxyl through the formation of bridging Al-O(H)-Pt bonds. In gas phase, only $\text{PtCl}_4(\text{H}_2\text{O})$ was expected to be stable.[58] Finally, the transition temperature between the $\text{PtCl}_y(\text{OH})_{4-y}(\text{H}_2\text{O})$ and the dehydrated species is around 200 K higher than in gas phase as it could be expected from the reaction energies values of the hydrations.

To check the sensitivity of our DFT results with the exchange-correlation functional, we report in **Figure S10** the calcination thermodynamic diagram calculated at the HSE06 level. As it was observed for the gas phase complexes,[58] both PBE-dDsC and HSE06 provide similar results as long as no changes of the oxidative degree are expected as it is the case for the calcination models. Without chlorine no change is observed, PtO_2 and $\text{Pt}(\text{OH})_4(\text{H}_2\text{O})$ are still expected and the transition is calculated at similar $(T, P(\text{H}_2\text{O}))$. Small changes are revealed for chlorinated species. The square planar PtOCl_2 is expected with PBE-dDsC at low HCl pressure ($P(\text{HCl}) = 1 \times 10^{-12}$ bar) at temperature between 400 K and 600 K for water pressure below 10^{-8} bar, whereas its domain is strongly shrunken in HSE06. The stabilization domain of PtOCl_2 increases at higher HCl pressure for water pressure ranging from 1×10^{-12} bar to 1×10^{-4} bar at 800 K for PBE-dDsC but only up to 1×10^{-6} bar in HSE06. Moreover, the very narrow stability domain of

PtOCl(OH) (a square planar species) which was found with PBE-dDsC is not visible in HSE06. Overall however, both functionals provide consistent results as it was already discussed in gas phase.[58]

4. Discussion

4.1 Comparison of DFT structures with EXAFS

The impact of chlorine on the coordination shell of platinum has been observed through EXAFS experiments as shown in section 3.2 for the two samples containing 0.1 and 1.4 wt% Cl. One Cl atom and five O atoms are found close to the platinum for 0.1 wt.% Cl against two Cl atoms and four O atoms at 1.4 wt.% Cl. For similar Pt loading (0.3 wt.%) and in the absence of chlorine, Dessal et al.[43] observed a coordination number of 5.5 ± 0.8 oxygens in the platinum first shell. Thus, the Pt species correspond to the octahedral complexes as predicted by DFT at low temperature.

In order to compare DFT and experiments, it has to be noticed that our samples as well as those by Dessal et al.[43] were cooled down at room temperature before analysis. We simulate this cooling down from a thermodynamic point of view in **Figure 7, a**. The water pressure is fixed at 1×10^{-6} bar (close to the experimental value) and as HCl pressure remains unknown during calcination, we allow it to range from 1×10^{-12} bar and 1 bar. Independently of the HCl content, below 500 K octahedral complexes $\text{PtCl}_y(\text{OH})_{4-y}(\text{H}_2\text{O})$ (with $y \geq 1$) are expected to be formed in place of PtO_2 , PtOCl_2 or PtCl_4 . As we observed here and in a previous work[7] dedicated to similar species but on different type of $\gamma\text{-Al}_2\text{O}_3$ support, even at the lowest chlorine amount considered, at least one Cl neighbour is expected. This observation is in agreement with the absence of the octahedral $\text{Pt}(\text{OH})_4(\text{H}_2\text{O})$ that could be expected from successive hydration of PtO_2 . However, from **Figure 6, a** in full absence of chlorine in the system, $\text{Pt}(\text{OH})_4(\text{H}_2\text{O})$ is

expected if calcined catalysts are cooled down. Thus, from a thermodynamic point of view, cooling down the sample before analysis is expected to change the supported species by stabilizing the five octahedral $\text{PtCl}_y(\text{OH})_{4-y}(\text{H}_2\text{O})$ species depending on the chlorine content in the system: $\text{PtCl}_4(\text{OH})\text{H}^*$, $\text{PtCl}_3(\text{OH})_2\text{H}^*$, $\text{PtCl}_2(\text{OH})_2(\text{H}_2\text{O})$, $\text{PtCl}(\text{OH})_3(\text{H}_2\text{O})$ and $\text{Pt}(\text{OH})_4(\text{H}_2\text{O})$.

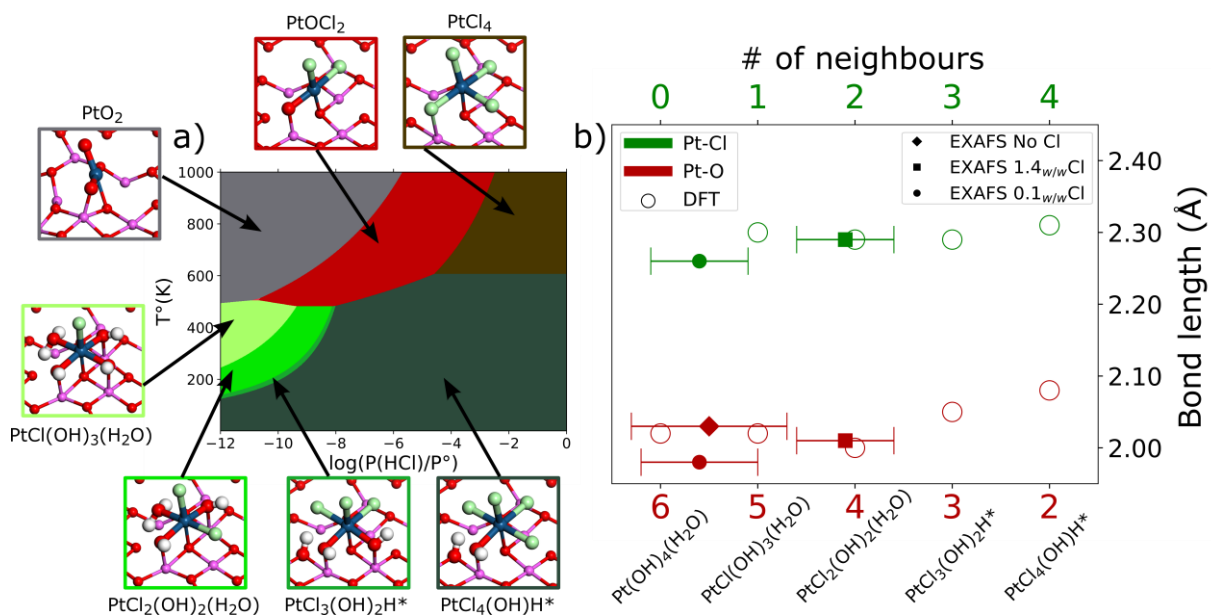


Figure 7. a) Thermodynamic diagram in which most stable species according to HCl pressure and temperature are depicted, for a water pressure fixed at 1×10^{-6} bar. b) Comparison of structural data obtained by EXAFS on 0.3 wt.%Pt calcined samples with various loading in chlorine, and by DFT models. The unchlorinated case (diamond symbol) was characterized by Dessal et al.[43] Plain symbols represent experimental values while empty ones represent DFT models. Bond lengths are plotted against the number and type of bonds in the Pt coordinative sphere with the top x-axis (in green) representing number of Cl neighbors to Pt, and the bottom x-axis (in red) representing the number of O neighbors to Pt. EXAFS values for chlorinated samples are taken from the fits done with aluminum in the second shell of Pt (Table 1).

The structural parameters of these five octahedral complexes are reported and compared to EXAFS results in **Figure 7, b**. Data corresponding to the chlorinated samples are reported in **Table 1**, while unchlorinated data are taken from the study of Dessal et al.[43] For the highest experimental amount of chlorine (1.4 wt%), $\text{PtCl}_2(\text{OH})_2(\text{H}_2\text{O})$ matches the best with both Pt-Cl and Pt-O coordination numbers and bond lengths. Experimentally, the coordination sphere of

platinum was fitted to be $N_{Pt-O} = 3.9 \pm 0.5$ and $N_{Pt-Cl} = 2.1 \pm 0.5$ with Pt-Cl and Pt-O distances fitted at 2.28 Å and 2.00 Å (**Table 1**) while DFT calculated average distances Pt-Cl and Pt-O bond lengths are calculated at 2.29 Å and 2.04 Å respectively (**Table S2**). For the low Cl loading (0.1 wt%), the simulated PtCl(OH)₃(H₂O) species agrees also well with EXAFS observations: the unique Pt-Cl bond is calculated at 2.30 Å by DFT and the mean Pt-O at 2.03 Å, while EXAFS reports $N_{Pt-O} = 5.2 \pm 0.6$ with Pt-O at 1.98 Å and $N_{Pt-Cl} = 0.8 \pm 0.6$ with Pt-Cl at 2.29 Å. The number of Cl atoms found as ligands of Pt is compatible with the chlorine contents of the two catalysts. The theoretical maximal Cl/Pt atomic ratios of ~1.9 and 26 for 0.1 wt% and 1.4 wt% Cl, respectively, knowing that part of the Cl atoms can be located on the alumina surface. Finally, without chlorine, N_{Pt-O} is estimated at 5.5 ± 0.8 and the mean Pt-O distance is 2.03 ± 0.03 Å, similarly as those calculated for Pt(OH)₄(H₂O) (2.02 Å). We thus identify 3 species of supported platinum complexes which are in good agreement with experimental observations: PtCl₂(OH)₂(H₂O) for 1.4 wt% Cl, PtCl(OH)₃(H₂O) for 0.1% Cl and Pt(OH)₄(H₂O) for the non-chlorinated sample.

Considering now the second coordination sphere, the comparison of the distance between platinum and the atoms of the second shell reveal that DFT Pt-O_{long} values are about 0.4 Å larger than EXAFS values (**Table 1** and **Table S4**). By contrast, DFT Pt-Al distances are much closer to EXAFS estimations: 2.99-3.16 Å and 2.91-2.95 Å, respectively (**Table S4**). Pt-Al coordination numbers (computed at 3) are also consistent. Thus, the most relevant EXAFS values are those obtained from the fit done with aluminum considered in the second shell.

To further compare the DFT models with EXAFS observations, we report in **Figure 8, a**) the FEFF simulation of the k^2 weighted magnitude of the Fourier transform (FT) of three different octahedral Pt complexes supported on the (100) γ -alumina surface: the fully chlorinated PtCl₄(OH)H^{*}, the fully hydroxylated Pt(OH)₄(H₂O) and the intermediate case

PtCl₂(OH)₂(H₂O). The analyses of the various paths for all octahedral species but PtCl₂(OH)₂(H₂O) (which is already exhibited in **Figure 8, b**) are displayed in **Figure S11**. In line with the previous analysis, we observe a reasonable agreement (both intensities and peak positions) with the FT spectra reported in **Figure 3, c** and **f**. We also notice a shift to higher radial distances for the first peak in the case of the PtCl₃(OH)₂H* and PtCl₄(OH)H* complexes in line with the increase of Cl neighbors.

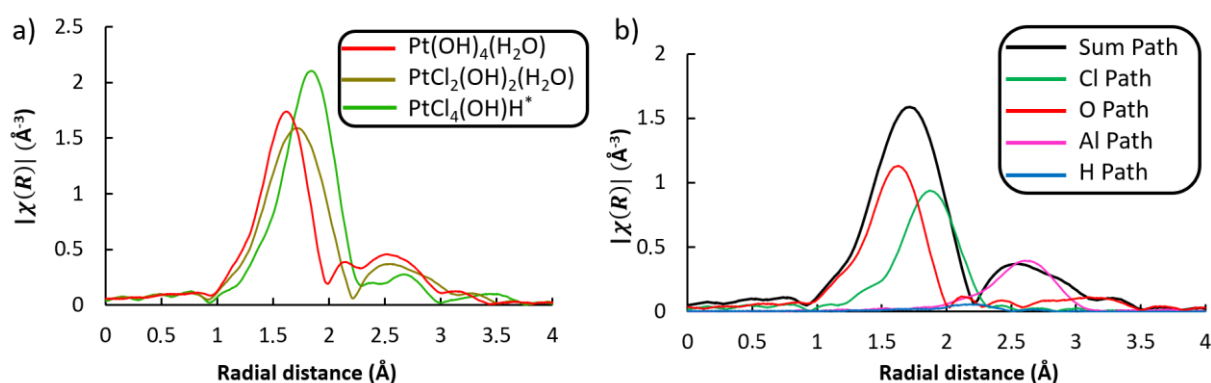


Figure 8. FEFF simulations of the k^2 weighted magnitude of the Fourier transform (FT). **a)** The sum of all paths is represented for the considered species, **b)** Decomposition of the paths for the PtCl₂(OH)₂(H₂O) species. Fits were performed over $\Delta k = 4\text{-}12\text{\AA}^{-1}$ and $\Delta R = 1.15\text{-}3.7\text{\AA}$.

The analysis of the various paths in the case of PtCl₂(OH)₂(H₂O) (**Figure 8, b**) reveals the distinct contributions of O and Cl atoms to the first peak of the sum while the second low intensity peak is mainly constituted from Pt-Al paths. By contrast Pt-O paths at large distances are more diffuse and may only contribute to the smaller peaks observed at larger radial distances (beyond 3 \AA in **Figure 3**). This is also supported by the representation of the imaginary part of the FEFF-simulated Fourier Transform which shows the predominance of Al signal in the 2.2-3 \AA region to the detriment of the O one (**Figure S12**). This confirms that the best EXAFS fit proposed in **Table 1** should be the one based on Pt-Al path which contributes to the second peak and not on Pt-O_{long}.

Moreover, as discussed in our previous DFT work,[58] no Pt-O bond and only Pt-Cl bonds were found in gas phase (unsupported) Pt complexes for similar analytical conditions (room temperature, $P(\text{H}_2\text{O})=1 \times 10^{-6}$ bar). The alumina support induces the stabilization of such Pt-O bonds through the formation of bridging Al-O(H)-Pt bonds. This result explains reasonably well why numerous EXAFS studies (including the present one) undertaken on alumina supported platinum materials report the joint existence of Pt-Cl and Pt-O bonds.[7,33,36,40,49,88,89]

4.2 Comparison of XANES simulation with HERDF-XANES experiments

XANES spectra have been simulated at the Pt L_3 -edge for all platinum complexes identified on the thermodynamic diagram. We report in **Figure 9** the simulated spectra for the octahedral $\text{PtCl}_y(\text{OH})_{4-y}(\text{H}_2\text{O})$ species identified from the first principle thermodynamic study reported above.

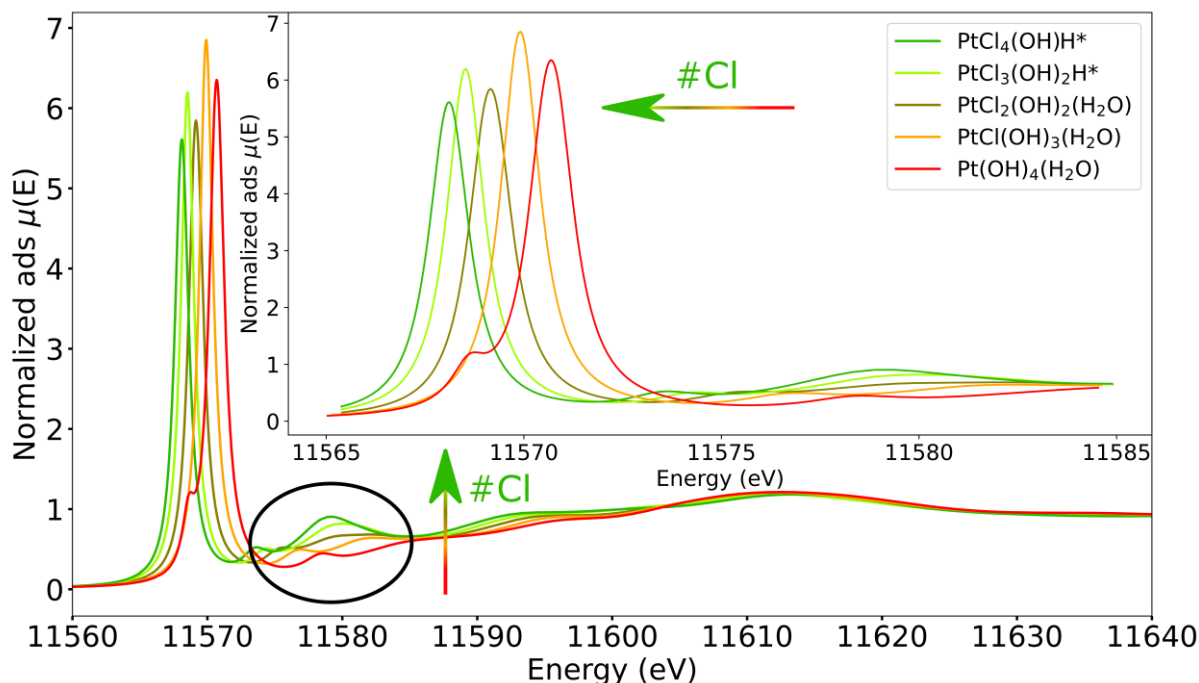


Figure 9. Calculated Pt L_3 -edge XANES spectra for various relevant octahedral $\text{PtCl}_y(\text{OH})_{4-y}(\text{H}_2\text{O})$ complexes. The two arrows represent the effect of ligands in the coordination sphere of Pt. The red

to green colors correspond to the evolution from a purely hydroxylated Pt complex to a fully chlorinated one.

Figure 9 reveals that as chlorine ligands are replaced by hydroxyls, a gradual shift of the WL toward the high energies is calculated (with the maximum of the WL calculated at 11569 eV for $\text{PtCl}_4(\text{OH})\text{H}^*$ and at 11571 eV for $\text{Pt}(\text{OH})_4(\text{H}_2\text{O})$ (**Table S5**)) in coherence with the increase of the positive charge of the platinum atom (**Figure 5**). This trend is also consistent with the one observed on the HERDF-XANES spectra (**Figure 2**), although the amplitude of the computed shift is too high. Simultaneously, the WL intensity is non-monotonously increased upon Cl/OH exchange. Overall, the WL intensities of these five species are in qualitative agreement with the WL of the experimental spectra (**Figure 9** and **Figure 10**), considering the accuracy of the simulation. More importantly, the spectral feature between 11575 eV and 11585 eV reproduces qualitatively well the trend observed in the experimental spectra, where a bump was revealed at 11580 eV for the high Cl content (**Figure 2**). This bump is obviously linked to the number of Cl atoms present in the coordination sphere of the Pt since we observe a gradual increase of the computed bump intensity in this region as the number of chlorine ligands (y) increases in $\text{PtCl}_y(\text{OH})_{4-y}(\text{H}_2\text{O})$ (**Figure 9**). This evolution is also observed for the other Pt $\text{PtCl}_y(\text{OH})_{4-y}$ species as illustrated in **Figure S15**.

In order to compare the simulated XANES more quantitatively to the experimental measurements of calcined Pt/ γ - Al_2O_3 for the two chlorine loadings (0.1 and 1.4 wt.%), we fitted the experimental spectra with a linear combination of all the octahedral $\text{PtCl}_y(\text{OH})_{4-y}(\text{H}_2\text{O})$ computed spectra by solving a least square problem. Indeed, one single species may not be sufficient to match well the experimental data. From these best fits, we aim at determining a quantified proportion of the species recovering the experimental HERFD-XANES spectra. However, due to the ground state nature of the DFT, that is used during the XANES calculation,

the WL area of the spectrum is not expected to be perfectly reproduced, even though reasonable agreements are obtained for heavy elements.[76] For this reason, we have attempted to fit calculated spectra for various interval of energies, including or excluding the WL region to probe the sensitivity of the proportion of the identified species (**Table S6**).

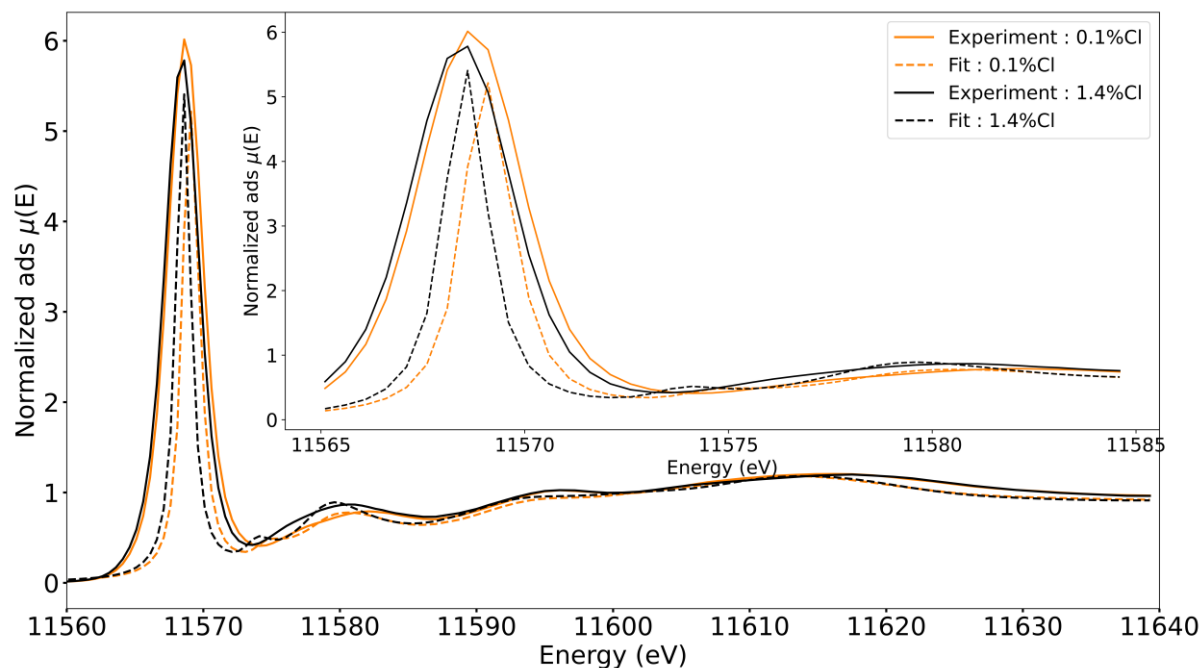


Figure 10. Comparison of experimental and FDMNES simulated XANES spectra. Pt L3-edge XANES spectra for the two calcined sample with 0.1 and 1.4 wt.% Cl appear in plain lines. The two simulated spectra obtained from the fitting of the $\text{PtCl}_y(\text{OH})_{4-y}(\text{H}_2\text{O})$ on the two references are in dashed lines. The fit was done for energies between 11575 eV and 11585 eV. $\text{PtCl}_y(\text{OH})_{4-y}(\text{H}_2\text{O})$ compositions corresponding to the fitted spectra are given in Table S6.

The corresponding fitted spectra over the range of energies corresponding to the 11575 eV – 11585 eV bump is reported in **Figure 10**. Even if **Table S6** shows that this quantification depends on the choice of the energy interval used (see **SI 12** for more details), we are able to propose a rather coherent trend for the proportion of each platinum complex after calcination. The fitted spectra (**Figure 10**) reproduce nicely the position and intensity of the WL as well as post WL features compared to experimental spectra. However, despite the combination of various spectra, the width of the WL remains underestimated compared to the experimental

one, while the bump at 11580 eV is qualitatively well reproduced. It is mandatory to consider a combination of 2 species ($\text{PtCl}_2(\text{OH})_2(\text{H}_2\text{O})$ with $\text{PtCl}_3(\text{OH})_2\text{H}^*$ for the 0.1%Cl content and $\text{PtCl}_3(\text{OH})_2\text{H}^*$ with $\text{PtCl}_4(\text{OH})\text{H}^*$ for the 1.4%Cl content) to reach the best fits in the 11575 eV – 11585 eV interval. From the evolution of the composition of the fitted spectra according to the two samples, the role of the chlorine on the feature between 11575 eV and 11585 eV seems thus undeniable. While exact compositions are reported in **Table S6**, the average number of Cl in the coordination sphere of platinum is evaluated at 2.7 Cl in the 0.1 wt.% Cl sample and 3.9 Cl for the reference at 1.4 wt.% Cl.

Independently of the domain of energies used for the fits, the trend remains similar and more chlorinated platinum complexes are identified during the fit of the spectrum of the 1.4 wt.% Cl sample than for the 0.1 wt.% Cl (**SI 12**). This confirms the EXAFS observation that the amount of chlorine in the platinum coordination sphere after calcination is impacted by the loading of chlorine used during the preparation. However, as the composition of the fitted spectra are highly sensitive to the domain used for the fit, we emphasize that these values coming from the composition of the fitted spectra to quantify the speciation of the $\text{PtCl}_y(\text{OH})_{4-y}(\text{H}_2\text{O})$ have to be considered with care. While the XANES spectra calculated from these octahedral platinum species are the closest to the experimental XANES spectra, XANES simulation of other non-octahedral $\text{PtCl}_y(\text{OH})_{4-y}$ species deviate more from experiments (**Figures S16**). This result is also coherent with the EXAFS results having shown that coordination number of Pt should be close to 6.

We finally notice that the XANES and EXAFS combined both with DFT simulations do not lead exactly to the same species. While EXAFS-DFT reveals the presence of $\text{PtCl}(\text{OH})_3(\text{H}_2\text{O})$ and $\text{PtCl}_2(\text{OH})_2(\text{H}_2\text{O})$ respectively for 0.1 and 1.4 wt.% Cl content, XANES-DFT suggests slightly higher Cl coordination with a combination of $\text{PtCl}_2(\text{OH})_2(\text{H}_2\text{O})$ and $\text{PtCl}_3(\text{OH})_2\text{H}^*$ in

the first case and a majority of $\text{PtCl}_4(\text{OH})\text{H}^*$ in the more chlorinated sample. This slight discrepancy can be tone down considering the fact that the two experimental techniques do not exactly probe in the same way the Pt environment and have also their own margin of errors. For instance, the fit of EXAFS coordination number is usually estimated within 20% of accuracy,[90] or even less considering the estimates made on our systems (**Table 1**), particularly for $N(\text{Pt-Cl})$. Simultaneously, the XANES fit is also subject to uncertainty due to some theoretical limitations in the treatment of excited states. However, being aware of the respective limitations of the two techniques, the analysis of the local environment of the Pt single atoms remains coherent as a function of chlorine contents.

5. Conclusion

The preparation from H_2PtCl_6 precursor of two samples of $\gamma\text{-Al}_2\text{O}_3$ supported Pt catalysts (0.3 wt% Pt) with two chlorine contents (0.1 and 1.4 wt%) and calcined (520 °C) allowed to generate mostly Pt single atom species with various Cl and O ligands depending on the chlorine content as identified by EXAFS and HERDF-XANES.

First principles thermodynamic diagrams have been calculated to determine the structures and the stability of the supported Pt single atoms during calcination (520 °C) and XAS experiments (after cooling down). The (T, P(H_2O)) conditions and Cl content impact the platinum coordination sphere. In comparison with previous results obtained on similar gas phase Pt species, the role of γ -alumina support is clearly highlighted. In the absence of chlorine, square planar PtO_2 complex (interacting through two Pt-O bonds with the support) is expected after calcination. Increasing Cl content stabilizes chlorinated Pt species such as square planar PtOCl_2 and square pyramidal PtCl_4 . In conditions corresponding to XAS analysis (room temperature), octahedral $\text{PtCl}_y(\text{OH})_{4-y}(\text{H}_2\text{O})$ species are found to be stabilized. Very low Cl amounts

transform $\text{Pt}(\text{OH})_4(\text{H}_2\text{O})$ (expected in absence of chlorine) into the hydroxy chlorinated $\text{PtCl}_y(\text{OH})_{4-y}(\text{H}_2\text{O})$ complexes.

According to EXAFS, the number of Cl neighbours to Pt is about 1 or 2 and the number of O atoms is about 5 or 4 respectively, while the total number of O and Cl atoms is close to 6. The octahedral $\text{PtCl}_y(\text{OH})_{4-y}(\text{H}_2\text{O})$ structures optimized by DFT calculations lead to a very good correspondence with EXAFS fitting results: for the weakly chlorinated catalysts, EXAFS is consistent with the $\text{PtCl}(\text{OH})_3(\text{H}_2\text{O})$ while for the highly chlorinated $\text{PtCl}_2(\text{OH})_2(\text{H}_2\text{O})$ is expected. Second shell Pt-Al distances are in good agreement between DFT models and EXAFS fits. XANES characterization reveals a bump feature above the whitenline (between 11575 eV and 11585 eV) which is sensitive to the chlorine content. By using the FDMNES code, the simulation of the XANES spectra of the octahedral $\text{PtCl}_y(\text{OH})_{4-y}(\text{H}_2\text{O})$ complexes highlighted that this remarkable bump feature is related to the amount of chlorine in the coordination sphere of the Pt. Fitting this region with the various possible $\text{PtCl}_y(\text{OH})_{4-y}(\text{H}_2\text{O})$ spectra revealed that the most probable species would be predominantly $\text{PtCl}_3(\text{OH})_2\text{H}^*$ with $\text{PtCl}_2(\text{OH})_2(\text{H}_2\text{O})$ and $\text{PtCl}_4(\text{OH})\text{H}^*$ with $\text{PtCl}_3(\text{OH})_2\text{H}^*$ depending on the Cl content.

Thus, thanks to a multi-technique approach, we go far beyond the previous state-of-art in terms of definition of the environment of the coordination sphere of platinum. Through pertinent DFT modelling of Pt complexes it is possible to better interpret XANES spectra and to comfort EXAFS fitting results in order to identify the local environment of Pt single atoms. This study provides a better understanding of the calcination step, opening the door to a better control of the genesis of the Pt SA on $\gamma\text{-Al}_2\text{O}_3$.

Acknowledgements

Calculations were performed using HPC resources (Jean Zay and Irene) from GENCI-CINES (Grant A0140806134) and ENER 440 from IFP Energies nouvelles. This work is part of the “RatiOnAl Design for CATalysis” (ROAD4CAT) industrial chair, project IDEXLYON funded by the French National Research Agency (ANR-16-IDEX-0005) and the Commissariat-General for Investment (CGI) within the framework of Investissements d’Avenir program (“Investment for the future”). The authors thank the SYSPROD project and AXELERA Pôle de Compétitivité for financial support (PSMN Data Center). The authors thank O. Ersen (ICPMS-CNRS-U. Strasbourg) and Anne-Lise Taleb (IFPEN) who have helped for the acquisition of HR-HAADF-STEM images at ICPMS. We thank F. Diehl (IFPEN) for fruitful discussions on the catalysts preparation.

References

- [1] P. Serp, D.P. Minh, Supported Metal Single Atom Catalysis, Wiley-VCH; Weinheim; Germany, 2022.
- [2] L. Liu, A. Corma, Metal Catalysts for Heterogeneous Catalysis: From Single Atoms to Nanoclusters and Nanoparticles, *Chem. Rev.* 118 (2018) 4981–5079.
- [3] A. Wang, J. Li, T. Zhang, Heterogeneous single-atom catalysis, *Nat. Rev. Chem.* 2 (2018) 65–81.
- [4] S.K. Kaiser, Z. Chen, D. Faust Akl, S. Mitchell, J. Pérez-Ramírez, Single-Atom Catalysts across the Periodic Table, *Chem. Rev.* 120 (2020) 11703–11809.
- [5] L. Piccolo, Restructuring effects of the chemical environment in metal nanocatalysis and single-atom catalysis, *Catal. Today* 373 (2021) 80–97.

- [6] A.T.F. Batista, C. Chizallet, F. Diehl, A.-L. Taleb, A.-S. Gay, O. Ersen, P. Raybaud, Evaluating acid and metallic site proximity in Pt/ γ -Al₂O₃-Cl bifunctional catalysts through an atomic scale geometrical model, *Nanoscale* 14 (2022) 8753–8765.
- [7] A.T.F. Batista, W. Baaziz, A.-L. Taleb, J. Chaniot, M. Moreaud, C. Legens, A. Aguilar-Tapia, O. Proux, J.-L. Hazemann, F. Diehl, C. Chizallet, A.-S. Gay, O. Ersen, P. Raybaud, Atomic Scale Insight into the Formation, Size, and Location of Platinum Nanoparticles Supported on γ -Alumina, *ACS Catal.* 10 (2020) 4193–4204.
- [8] P. Munnik, P.E. de Jongh, K.P. de Jong, Recent developments in the synthesis of supported catalysts, *Chem. Rev.* 115 (2015) 6687–6718.
- [9] A. Chen, P. Holt-Hindle, Platinum-based nanostructured materials: synthesis, properties, and applications, *Chem. Rev.* 110 (2010) 3767–3804.
- [10] J. Finzel, K.M. Sanroman Gutierrez, A.S. Hoffman, J. Resasco, P. Christopher, S.R. Bare, Limits of Detection for EXAFS Characterization of Heterogeneous Single-Atom Catalysts, *ACS Catal.* (2023) 6462–6473.
- [11] V. Haensel, Alumina-Platinum-Halogen Catalyst And Preparation Thereof. U.S. Patent 2,479,109, 2,479,109 (1949), Universal Oil Product.
- [12] R.J. Farrauto, R.M. Heck, Catalytic converters: state of the art and perspectives, *Catal. Today* 51 (1999) 351–360.
- [13] G.W. Huber, R.D. Cortright, J.A. Dumesic, Renewable alkanes by aqueous-phase reforming of biomass-derived oxygenates, *Angew. Chem. Int. Ed.* 43 (2004) 1549–1551.
- [14] J.J.H.B. Sattler, J. Ruiz-Martinez, E. Santillan-Jimenez, B.M. Weckhuysen, Catalytic dehydrogenation of light alkanes on metals and metal oxides, *Chem. Rev.* 114 (2014) 10613–10653.

- [15] F. Zhang, M. Zeng, R.D. Yappert, J. Sun, Y.-H. Lee, A.M. LaPointe, B. Peters, M.M. Abu-Omar, S.L. Scott, Polyethylene upcycling to long-chain alkylaromatics by tandem hydrogenolysis/aromatization, *Science* 370 (2020) 437–441.
- [16] G. Ertl, H. Knözinger, F. Schüth, J. Weitkamp (Eds.), *Handbook of Heterogeneous Catalysis*, 2nd ed., Wiley-VCH; Weinheim; Germany, 2008.
- [17] A.N. Jahel, V. Moizan-Baslé, C. Chizallet, P. Raybaud, J. Olivier-Fourcade, J.-C. Jumas, P. Avenier, S. Lacombe, Effect of Indium Doping of γ -Alumina on the Stabilization of PtSn Alloyed Clusters Prepared by Surface Organostannic Chemistry, *J. Phys. Chem. C* 116 (2012) 10073–10083.
- [18] E.J. Jang, J. Lee, H.Y. Jeong, J.H. Kwak, Controlling the acid-base properties of alumina for stable PtSn-based propane dehydrogenation catalysts, *Appl. Catal. A* 572 (2019) 1–8.
- [19] W. Karim, C. Spreatico, A. Kleibert, J. Gobrecht, J. VandeVondele, Y. Ekinici, J.A. van Bokhoven, Catalyst support effects on hydrogen spillover, *Nature* 541 (2017) 68–71.
- [20] J.H. Sinfelt, Catalysis by alloys and bimetallic clusters, *Acc. Chem. Res.* 10 (1977) 15–20.
- [21] W. Yu, M.D. Porosoff, J.G. Chen, Review of Pt-based bimetallic catalysis: from model surfaces to supported catalysts, *Chem. Rev.* 112 (2012) 5780–5817.
- [22] R. Burch, Platinum-tin reforming catalysts I. The oxidation state of tin and the interaction between platinum and tin, *J. Catal.* 71 (1981) 348–359.
- [23] A. Rocherfort, Particle size effect in supported platinum: Methylcyclohexane dehydrogenation, *J. Catal.* 138 (1992) 482–490.
- [24] E. Marceau, X. Carrier, M. Che, Impregnation and Drying, in: K.P. de Jong (Ed.), *Synthesis of Solids Catalysts*, Wiley-VCH Verlag GmbH & Co. KGaA, Weinheim, Germany, 2009, pp. 59–82.

- [25] G.J. Antos, A.M. Aitani (Eds.), Catalytic naphtha reforming, 2nd ed., Marcel Dekker, New York, 2004.
- [26] J.T. García-Sánchez, V.G. Baldovino-Medrano, Elements of the Manufacture and Properties of Technical Catalysts, *Ind. Eng. Chem. Res.* (2023).
- [27] B. Shelimov, J.F. Lambert, M. Che, B. Didillon, Initial Steps of the Alumina-Supported Platinum Catalyst Preparation: A Molecular Study by ^{195}Pt NMR, UV–Visible, EXAFS, and Raman Spectroscopy, *J. Catal.* 185 (1999) 462–478.
- [28] J.H. Sinfelt, Catalytic reforming, in: G. Ertl, H. Knözinger, F. Schüth, J. Weitkamp (Eds.), *Handbook of Heterogeneous Catalysis*, 2nd ed., Wiley-VCH; Weinheim; Germany, 1997, p. 1939.
- [29] P. Avenier, D. Bazer-Bachi, F. Bazer-Bachi, C. Chizallet, F. Deleau, F. Diehl, J. Gornay, É. Lemaire, V. Moizan-Basle, C. Plais, P. Raybaud, F. Richard, S. Lacombe, Catalytic Reforming: Methodology and Process Development for a Constant Optimisation and Performance Enhancement, *Oil Gas Sci. Technol. – Rev. IFP Energies nouvelles* 71 (2016) 41.
- [30] P.-Y. Le Goff, W. Kostka, J. Ross, Catalytic Reforming, in: C.S. Hsu, P.R. Robinson (Eds.), *Springer Handbook of Petroleum Technology*, Springer International Publishing, Cham, 2017, pp. 589–616.
- [31] M. Digne, P. Raybaud, P. Sautet, D. Guillaume, H. Toulhoat, Atomic scale insights on chlorinated gamma-alumina surfaces, *J. Am. Chem. Soc.* 130 (2008) 11030–11039.
- [32] J.H. Sinfelt, Bifunctional Catalysis, in: *Advances in Chemical Engineering Volume 5*, Elsevier, 1964, pp. 37–74.
- [33] Berdala, J., Freund, E., Lynch J. P., Environment of platinum atoms in a $\text{H}_2\text{PtCl}_6/\text{Al}_2\text{O}_3$ catalyst Influence of metal loading and chlorine content, *J. Phys. Colloques* 47 (1986) C8-269-C8-272.

- [34] J.P. Franck, G. Martino, Deactivation and Regeneration of Catalytic-Reforming Catalysts, in: J.L. Figueiredo (Ed.), Progress in Catalyst Deactivation, Springer-Verlag, Dordrecht, 1982, pp. 355–397.
- [35] F. Le Normand, A. Borgna, T.F. Garetto, C.R. Apesteguia, B. Moraweck, Redispersión of Sintered Pt/Al₂O₃ Naphtha Reforming Catalysts: An in Situ Study Monitored by X-ray Absorption Spectroscopy, *J. Phys. Chem.* 100 (1996) 9068–9076.
- [36] K. Morgan, A. Goguet, C. Hardacre, Metal Redispersión Strategies for Recycling of Supported Metal Catalysts: A Perspective, *ACS Catal.* 5 (2015) 3430–3445.
- [37] D.A. Svintsitskiy, L.S. Kibis, A.I. Stadnichenko, E.M. Slavinskaya, A.V. Romanenko, E.A. Fedorova, O.A. Stonkus, D.E. Doronkin, V. Marchuk, A. Zimina, M. Casapu, J.D. Grunwaldt, A.I. Boronin, Insight into the Nature of Active Species of Pt/Al₂O₃ Catalysts for low Temperature NH₃ Oxidation, *ChemCatChem* 12 (2020) 867–880.
- [38] E. Marceau, H. Lauron-Pernot, M. Che, Influence of the Metallic Precursor and of the Catalytic Reaction on the Activity and Evolution of Pt(Cl)/ δ -Al₂O₃ Catalysts in the Total Oxidation of Methane, *J. Catal.* 197 (2001) 394–405.
- [39] E. Marceau, M. Che, J. Saint-Just, J.M. Tatibouët, Influence of chlorine ions in Pt/Al₂O₃ catalysts for methane total oxidation, *Catal. Today* 29 (1996) 415–419.
- [40] F.J. Gracia, J.T. Miller, A.J. Kropf, E.E. Wolf, Kinetics, FTIR, and Controlled Atmosphere EXAFS Study of the Effect of Chlorine on Pt-Supported Catalysts during Oxidation Reactions, *J. Catal.* 209 (2002) 341–354.
- [41] H. Yao, M. Sieg, H. Plummerjr, Surface interactions in the Pt/-AlO system, *J. Catal.* 59 (1979) 365–374.
- [42] C. Dessal, T. Len, F. Morfin, J.L. Rousset, M. Aouine, P. Afanasiev, L. Piccolo, Dynamics of Single Pt Atoms on Alumina during CO Oxidation Monitored by Operando X-ray and Infrared Spectroscopies, *ACS Catal.* 9 (2019) 5752–5759.

- [43] C. Dessal, A. Sangnier, C. Chizallet, C. Dujardin, F. Morfin, J.L. Rousset, Aouine, M. Bugnet, M., P. Afanasiev, L. Piccolo, Atmosphere-dependent stability and mobility of catalytic Pt single atoms and clusters on γ -Al₂O₃, *Nanoscale* 11 (2019) 6897–6904.
- [44] S.A. Bradley, W. Sinkler, D.A. Blom, W. Bigelow, P.M. Voyles, L.F. Allard, Behavior of Pt Atoms on Oxide Supports During Reduction Treatments at Elevated Temperatures, Characterized by Aberration Corrected Stem Imaging, *Catal. Lett.* 142 (2012) 176–182.
- [45] J. Lee, E.J. Jang, D.G. Oh, J. Szanyi, J.H. Kwak, Morphology and size of Pt on Al₂O₃: The role of specific metal-support interactions between Pt and Al₂O₃, *J. Catal.* 385 (2020) 204–212.
- [46] J.F. Lambert, E. Marceau, B. Shelimov, J. Lehman, V. Le Bel de Penguilly, X. Carrier, S. Boujday, H. Pernot, M. Che, Thermal chemistry of oxide-supported platinum catalysts: A comparative study, *Stud. Sci. Surf. Catal.* 130 (2000) 1043–1048.
- [47] M.G.V. Mordente, C.H. Rochester, Infrared study of the effects of oxychlorination on Pt dispersion in Pt/Al₂O₃ catalysts, *J. Chem. Soc., Faraday Trans. 1* 85 (1989) 3495.
- [48] Y. Zhou, M. Wood, N. Winograd, A time-of-flight SIMS study of the chemical nature of highly dispersed Pt on alumina, *J. Catal.* 146 (1994) 82–86.
- [49] H. Lieske, Reactions of platinum in oxygen- and hydrogen-treated Pt/ γ -Al₂O₃ catalysts I. Temperature-programmed reduction, adsorption, and redispersion of platinum, *J. Catal.* 81 (1983) 8–16.
- [50] G. Lietz, Reactions of platinum in oxygen- and hydrogen-treated Pt/ γ -Al₂O₃ catalysts II. Ultraviolet-visible studies, sintering of platinum, and soluble platinum, *J. Catal.* 81 (1983) 17–25.
- [51] T. Cholley, Etude de la redispersion de phase bimétallique à base de platine supportées sur alumine chlorée ou neutralisée. PhD, IFP Energies nouvelles, 1997.

- [52] W. Kohn, L.J. Sham, Self-Consistent Equations Including Exchange and Correlation Effects, *Phys. Rev.* 140 (1965) A1133-A1138.
- [53] P. Hohenberg, W. Kohn, Inhomogeneous Electron Gas, *Phys. Rev.* 136 (1964) B864-B871.
- [54] C. Chizallet, P. Raybaud, Density functional theory simulations of complex catalytic materials in reactive environments: beyond the ideal surface at low coverage, *Catal. Sci. Technol.* 4 (2014) 2797–2813.
- [55] C. Chizallet, Achievements and Expectations in the Field of Computational Heterogeneous Catalysis in an Innovation Context, *Top. Catal.* 65 (2022) 69–81.
- [56] M. Shahrokhi, C. Chizallet, D. Loffreda, P. Raybaud, Stability of Pt₁₀Sn₃ Clusters Supported on γ -Al₂O₃ in Oxidizing Environment: a DFT Comparison of Alloying and Size Effects, *ChemCatChem* 14 (2022) e202201089.
- [57] A. Sangnier, M. Matrat, A. Nicolle, C. Dujardin, C. Chizallet, Multiscale Approach to the Dissociative Adsorption of Oxygen on a Highly Dispersed Platinum Supported on γ -Al₂O₃, *J. Phys. Chem. C* 122 (2018) 26974–26986.
- [58] A. Hellier, C. Chizallet, P. Raybaud, PtO_xCl_y(OH)_z(H₂O)_n Complexes under Oxidative and Reductive Conditions: Impact of the Level of Theory on Thermodynamic Stabilities, *ChemphysChem* (2023) 24, e202200711.
- [59] X. Zhou, Y. Zhang, J. Wang, DFT study on the regeneration of Pt/ γ -Al₂O₃ catalyst: The effect of chlorine on the redispersion of metal species, *Appl. Surf. Sci.* 545 (2021) 148988.
- [60] O. Proux, E. Lahera, W. Del Net, I. Kieffer, M. Rovezzi, D. Testemale, M. Irar, S. Thomas, A. Aguilar-Tapia, E.F. Bazarkina, A. Prat, M. Tella, M. Auffan, J. Rose, J.L. Hazemann, High-Energy Resolution Fluorescence Detected X-Ray Absorption

- Spectroscopy: A Powerful New Structural Tool in Environmental Biogeochemistry Sciences, *J. Environ. Qual.* 46 (2017) 1146–1157.
- [61] B. Ravel, M. Newville, Athena, Artemis, Hephæstus: data analysis for X-ray absorption spectroscopy using IFEFFIT, *J. Synchrotron Radiat.* 12 (2005) 537–541.
- [62] G. Kresse, J. Hafner, Ab initio molecular-dynamics simulation of the liquid-metal-amorphous-semiconductor transition in germanium, *Phys. Rev. B* 49 (1994) 14251–14269.
- [63] G. Kresse, J. Furthmüller, Efficiency of ab-initio total energy calculations for metals and semiconductors using a plane-wave basis set, *Comput. Mater. Sci.* 6 (1996) 15–50.
- [64] J.P. Perdew, K. Burke, M. Ernzerhof, Generalized Gradient Approximation Made Simple, *Phys. Rev. Lett.* 77 (1996) 3865–3868.
- [65] S.N. Steinmann, C. Corminboeuf, A generalized-gradient approximation exchange hole model for dispersion coefficients, *J. Chem. Phys.* 134 (2011) 44117.
- [66] S.N. Steinmann, C. Corminboeuf, Comprehensive Benchmarking of a Density-Dependent Dispersion Correction, *J. Chem. Theory Comput.* 7 (2011) 3567–3577.
- [67] G. Kresse, D. Joubert, From ultrasoft pseudopotentials to the projector augmented-wave method, *Phys. Rev. B* 59 (1999) 1758–1775.
- [68] F.L. Hirshfeld, Bonded-atom fragments for describing molecular charge densities, *Theoret. Chim. Acta* 44 (1977) 129–138.
- [69] J. Heyd, G.E. Scuseria, Efficient hybrid density functional calculations in solids: assessment of the Heyd-Scuseria-Ernzerhof screened Coulomb hybrid functional, *J. Chem. Phys.* 121 (2004) 1187–1192.
- [70] J. Heyd, G.E. Scuseria, M. Ernzerhof, Hybrid functionals based on a screened Coulomb potential, *J. Chem. Phys.* 118 (2003) 8207–8215.

- [71] A.V. Krukau, O.A. Vydrov, A.F. Izmaylov, G.E. Scuseria, Influence of the exchange screening parameter on the performance of screened hybrid functionals, *J. Chem. Phys.* 125 (2006) 224106.
- [72] M. Digne, P. Sautet, P. Raybaud, P. Euzen, H. Toulhoat, Hydroxyl Groups on γ -Alumina Surfaces: A DFT Study, *J. Catal.* 211 (2002) 1–5.
- [73] M. Digne, Use of DFT to achieve a rational understanding of acid basic properties of gamma-alumina surfaces, *J. Catal.* 226 (2004) 54–68.
- [74] X. Krokidis, P. Raybaud, A.E. Gobichon, B. Rebours, P. Euzen, H. Toulhoat, Theoretical Study of the Dehydration Process of Boehmite to γ -Alumina, *J. Phys. Chem. B* 105 (2001) 5121–5130.
- [75] T. Pigeon, C. Chizallet, P. Raybaud, Revisiting γ -alumina surface models through the topotactic transformation of boehmite surfaces, *J. Catal.* 405 (2022) 140–151.
- [76] O. Bunău, Y. Joly, Self-consistent aspects of x-ray absorption calculations, *J. Phys.: Condens. Matter* 21 (2009) 345501.
- [77] O. Bunău, A.Y. Ramos, Y. Joly, The FDMNES code, *International tables for crystallography - X-ray Absorption I* (2021).
- [78] L. Hedin, B.I. Lundqvist, Explicit local exchange-correlation potentials, *J. Phys. C: Solid State Phys.* 4 (1971) 2064–2083.
- [79] Y. Joly, X-ray absorption near-edge structure calculations beyond the muffin-tin approximation, *Phys. Rev. B* 63 (2001).
- [80] S. Diamond, S. Boyd, CVXPY: A Python-Embedded Modeling Language for Convex Optimization, *JMLR* 17 (2016).
- [81] A. Agrawal, R. Verschueren, S. Diamond, S. Boyd, A rewriting system for convex optimization problems, *JCD* 5 (2018) 42–60.

- [82] M. Muñoz, P. Argoul, F. Farges, Continuous Cauchy wavelet transform analyses of EXAFS spectra: A qualitative approach, *Am. Min.* 88 (2003) 694–700.
- [83] M.K. Oudenhuijzen, J.H. Bitter, D.C. Koningsberger, The Nature of the Pt–H Bonding for Strongly and Weakly Bonded Hydrogen on Platinum. A XAFS Spectroscopy Study of the Pt–H Antibonding Shaperesonance and Pt–H EXAFS, *J. Phys. Chem. B* 105 (2001) 4616–4622.
- [84] A. Munoz-Paez, D.C. Koningsberger, Decomposition of the Precursor $[\text{Pt}(\text{NH}_3)_4](\text{OH})_2$, Genesis and Structure of the Metal-Support Interface of Alumina Supported Platinum Particles: A Structural Study Using TPR, MS, and XAFS Spectroscopy, *J. Phys. Chem.* 99 (1995) 4193–4204.
- [85] D. Mei, J.H. Kwak, J. Hu, S.J. Cho, J. Szanyi, L.F. Allard, C.H.F. Peden, Unique Role of Anchoring Penta-Coordinated Al^{3+} Sites in the Sintering of $\gamma\text{-Al}_2\text{O}_3$ -Supported Pt Catalysts, *J. Phys. Chem. Lett.* 1 (2010) 2688–2691.
- [86] X. Cui, K. Junge, X. Dai, C. Kreyenschulte, M.M. Pohl, S. Wohlrab, F. Shi, A. Brückner, M. Beller, Synthesis of Single Atom Based Heterogeneous Platinum Catalysts: High Selectivity and Activity for Hydrosilylation Reactions, *ACS central science* 3 (2017) 580–585.
- [87] P. Raybaud, M. Digne, R. Iftimie, W. Wellens, P. Euzen, H. Toulhoat, Morphology and Surface Properties of Boehmite ($\gamma\text{-AlOOH}$): A Density Functional Theory Study, *J. Catal* 201 (2001) 236–246.
- [88] A. Borgna, F. Le Normand, T. Garetto, C.R. Apesteguia, B. Moraweck, Sintering of Pt/ Al_2O_3 reforming catalysts: EXAFS study of the behavior of metal particles under oxidizing atmosphere, *Catal. Lett.* 13 (1992) 175–188.
- [89] P. Lagarde, EXAFS studies of Pt/ Al_2O_3 catalysts, *J. Catal.* 84 (1983) 333–343.

- [90] G.G. Li, F. Bridges, C.H. Booth, X-ray-absorption fine-structure standards: A comparison of experiment and theory, *Phys. Rev. B* 52 (1995) 6332–6348.